Pergamon

Atmospheric Environment Vol. 29, No. 4, pp. 479–496, 1995
Elsevier Science Ltd
Printed in Great Britain

1352–2310(94)00279–7

NUMERICAL INVESTIGATION OF POSSIBLE ROLE OF LOCAL METEOROLOGY IN BHOPAL GAS ACCIDENT

ZAFER BOYBEYI* and SETHU RAMAN
Department of Marine, Earth and Atmospheric Sciences, North Carolina State University, Raleigh, NC 27695-8208, U.S.A.

and

PAOLO ZANNETTI
Failure Analysis Associates, Inc., 149 Commonwealth Drive, P.O. Box 3015, Menlo Park, CA 94025, U.S.A.

(*First received* 30 *December* 1992 *and in final form* 2 *August* 1994)

Abstract—Two numerical models were coupled in this study; a three-dimensional mesoscale meteorological model and a three-dimensional Monte Carlo dispersion model. The dispersion of methyl isocyanate gas from the Bhopal accident was examined using the coupled models. A series of numerical experiments were performed to investigate the possible role of the surface induced mesoscale circulations and various environmental parameters on this industrial gas episode. The temporal and spatial variations of the wind and turbulence fields were simulated by the mesoscale model. The dispersion of the accidentally released methyl isocyanate gas was then evaluated by the Monte Carlo model using these wind and turbulence fields. The numerical experiments suggest that the reported complex dispersion of the gas at Bhopal could have resulted from the interaction of thermally forced mesoscale circulations. Results especially point to the effect of the Bhopal urban heat island which dominated the local circulation and trapped the gas over Bhopal city. The calm ambient winds, clear skies, and stable nocturnal atmospheric conditions that prevailed during the accident are consistent with the formation of an urban heat island effect over Bhopal.

Key word index: Mesoscale modeling, air pollution, Lagrangian particle dispersion, Monte Carlo technique, urban heat island, coupled model, Bhopal gas accident.

1. INTRODUCTION

Over the past decade, there has been increasing interest in evaluating air pollution episodes associated with accidental toxic gas and radioactive releases. These releases can cause serious health hazards and even fatalities, such as the ones that occurred with the chemical release in Bhopal, India, the radioactive emissions from the Chernobyl nuclear power station in the former Soviet Union, and recently the smoke plumes from the Kuwaiti oil well fires. Undoubtedly, the role of meteorology in all air pollution episodes is of pivotal importance, since the movement of pollutants in the atmosphere is governed by atmospheric motion. It is, therefore, essential to use detailed meteorological information in the dispersion models to improve our understanding of the transport and diffusion of air pollutants. Such detailed meteorological information can be obtained either from interpolated meteorological observations or meteorological models.

Until recently, observations have been used to obtain necessary meteorological information for dispersion models (e.g. Pack *et al.*, 1978; Artz *et al.*, 1985). These studies, however, have demonstrated that the observations are too coarse in both time and space to accurately depict local circulations. Small scale features of the wind and turbulence fields are neglected in these models. This loss of resolution is especially serious where the temporal and spatial inhomogeneities of the wind and turbulence fields are significant.

One approach to overcome the limitation of the existing meteorological observations is to use the information predicted by meteorological models. For example, Bornstein *et al.* (1987a, b) coupled a mesoscale meteorological model with an Eulerian gridded dispersion model in order to study the urban boundary layer structure of New York City. The meteorological model provided the velocity and vertical diffusivity fields. Results demonstrated that the coupled models could simulate most of the features of the polluted urban boundary layer during sea breeze

* Present affiliation: SAIC, 1710 Goodridge Drive, McLean, VA 22102, U.S.A.

conditions. One limitation in their study, however, was the treatment of near stack dispersion using point sources. This is a general problem for all Eulerian dispersion models due to the homogeneous grid cells. The problem results from the limited spatial resolution of such models. In many cases, plumes or puffs initially occupy a volume smaller than the size of one dispersion model grid cell, and do not expand to fill a cell until far downwind.

The characteristics of localized emissions can be simulated better by coupling meteorological models with Lagrangian dispersion models. Such coupling does not suffer from numerical problems associated with the grid size resolution. Transport terms, whose correct numerical treatment of subgrid scale plumes or puffs is very difficult with Eulerian gridded models, are handled in a straightforward manner in the Lagrangian models. For example, one such coupling was accomplished by McNider *et al.* (1988), who studied the influence of diurnal variation and inertial boundary-layer oscillations on long-range dispersion. Another coupling was made by Pitts and Lyons (1992) with an application to the urban area of Perth, Australia. Their model results satisfactorily reproduced the magnitudes and spread of the plume. These and other studies have demonstrated that Lagrangian particle dispersion models can successfully simulate turbulent fluid dynamics in a wide spectrum of applications.

In this study two numerical models were coupled. One is a three-dimensional mesoscale meteorological model that provides detailed meteorological information. The other is a three-dimensional Monte Carlo dispersion model that simulates dispersion of pollutant emissions through the use of the wind and turbulence fields obtained from the mesoscale model fields. The dispersion of methyl isocyanate gas from the Bhopal accident was then examined using the coupled models. The primary objective of this study is to investigate the possible role of the surface induced mesoscale circulations and various environmental parameters on the dispersion of the accidentally released methyl isocyanate gas.

2. METHODOLOGY

Methodology of the study and description of the coupled models are summarized below.

2.1. *Mesoscale meteorological model*

The mesoscale model used in this study is described in detail by Huang and Raman (1990, 1991) and similar to that used in Boybeyi and Raman (1992a, b). Thus, only a brief description of the model is given here. The model is hydrostatic and anelastic in a terrain-following coordinate system. The governing equations for the mean variables are

$$\frac{\partial u}{\partial t} = -u\frac{\partial u}{\partial x} - v\frac{\partial u}{\partial y} - \tilde{w}\frac{\partial u}{\partial \sigma} + fv - \theta_v\frac{\partial \pi}{\partial x} - g(1-\sigma)\frac{\partial \hat{E}}{\partial x} + \frac{\partial}{\partial x}\left(K_H\frac{\partial u}{\partial x}\right) + \frac{\partial}{\partial y}\left(K_H\frac{\partial u}{\partial y}\right) + \frac{1}{H-\hat{E}}\frac{\partial}{\partial \sigma}(\overline{-u'w'}), \quad (1)$$

$$\frac{\partial v}{\partial t} = -u\frac{\partial v}{\partial x} - v\frac{\partial v}{\partial y} - \tilde{w}\frac{\partial v}{\partial \sigma} - fu - \theta_v\frac{\partial \pi}{\partial y} - g(1-\sigma)\frac{\partial \hat{E}}{\partial y} + \frac{\partial}{\partial x}\left(K_H\frac{\partial v}{\partial x}\right) + \frac{\partial}{\partial y}\left(K_H\frac{\partial v}{\partial y}\right) + \frac{1}{H-\hat{E}}\frac{\partial}{\partial \sigma}(\overline{-v'w'}), \quad (2)$$

$$\frac{\partial \theta}{\partial t} = -u\frac{\partial \theta}{\partial x} - v\frac{\partial \theta}{\partial y} - \tilde{w}\frac{\partial \theta}{\partial \sigma} + \frac{\partial}{\hat{c}x}\left(K_H\frac{\partial \theta}{\partial x}\right) + \frac{\partial}{\partial y}\left(K_H\frac{\partial \theta}{\partial y}\right) + \frac{1}{H-\hat{E}}\frac{\hat{c}}{\hat{c}\sigma}(\overline{-w'\theta'}) - \frac{L_c}{\pi}\left(\delta\frac{dq_s}{dt}\right) + Q_{CL} - Q_{EV} + Q_{RAD}, \quad (3)$$

$$\frac{\partial q}{\partial t} = -u\frac{\partial q}{\partial x} - v\frac{\partial q}{\partial y} - \tilde{w}\frac{\partial q}{\partial \sigma} + \frac{\partial}{\hat{c}x}\left(K_H\frac{\partial q}{\partial x}\right) + \frac{\partial}{\partial y}\left(K_H\frac{\partial q}{\partial y}\right) + \frac{1}{H-\hat{E}}\frac{\hat{c}}{\hat{c}\sigma}(\overline{-w'q'}) + \delta\frac{dq_s}{dt} + M_{CL} + M_{EV}, \quad (4)$$

$$\frac{\partial q_c}{\partial t} = -u\frac{\partial q_c}{\partial x} - v\frac{\partial q_c}{\partial y} - \tilde{w}\frac{\partial q_c}{\partial \sigma} + \frac{\partial}{\partial x}\left(K_H\frac{\hat{c}q_c}{\hat{c}x}\right) + \frac{\partial}{\partial y}\left(K_H\frac{\partial q_c}{\partial y}\right) + \frac{1}{H-\hat{E}}\frac{\partial}{\partial \sigma}(\overline{-w'q_c'}) - \delta\frac{dq_s}{dt} - M_{AC} - M_{RV}, \quad (5)$$

$$\frac{\partial q_r}{\partial t} = -u\frac{\partial q_r}{\partial x} - v\frac{\partial q_r}{\partial y} - \tilde{w}\frac{\partial q_r}{\partial \sigma} + \frac{\partial}{\partial x}\left(K_H\frac{\hat{c}q_r}{\hat{c}x}\right) + \frac{\partial}{\partial y}\left(K_H\frac{\partial q_r}{\partial y}\right) + \frac{1}{H-\hat{E}}\frac{\partial}{\partial \sigma}(\overline{-w'q_r'}) + M_{VT} + M_{AC} + M_{RV} - M_{EV}, \quad (6)$$

$$\frac{\partial \rho u(H-\hat{E})}{\partial x} + \frac{\partial \rho v(H-\hat{E})}{\partial y} + \frac{\partial \rho \tilde{w}(H-\hat{E})}{\hat{c}\sigma} = 0, \quad (7)$$

$$\frac{\partial \pi}{\partial \sigma} = -\frac{g(H-\hat{E})}{\theta_v}, \quad (8)$$

where the terrain-following coordinate is defined as

$$\sigma = \frac{z-\hat{E}}{H-\hat{E}}, \quad (9)$$

using the maximum height of the model domain, H, and the terrain height, $\hat{E}$. Equations (1) and (2) are the horizontal momentum (u and v) equations for east–west and north–south directions, respectively. Equation (3) is the thermodynamic energy equation for the potential temperature (θ). Equations (4)–(6) are the conservation equations for water vapor (q), cloud water (q_c) and rain water (q_r), respectively. Equation (7) is the anelastic equation for fluid continuity. Equation (8) is the hydrostatic equation.

The scaled pressure, π, from the Exner function is defined as

$$\pi = c_p\left(\frac{p}{p_{00}}\right)^{\kappa}, \quad \kappa = \frac{R}{c_p}, \quad (10)$$

where p is pressure with the reference pressure, p_{00}, set to 1000 mb. The virtual potential temperature, θ_v, is defined as

$$\theta_v = \theta(1 + 0.61\,q - q_c - q_r). \quad (11)$$

The vertical velocity in the σ-coordinate, $\tilde{w}$, is related to vertical velocity in the z-coordinate, w, by

$$w = \tilde{w}(H-\hat{E}) - (\sigma-1)\left(u\frac{\hat{c}\hat{E}}{\hat{c}x} + v\frac{\partial \hat{E}}{\partial y}\right). \quad (12)$$

The sink or source terms in equations (3)–(6) are described in detail by Huang and Raman (1990).

The atmospheric planetary boundary layer is treated in two parts as the surface layer and the transition layer. The surface layer turbulent transport is based upon the similarity

stability functions given by Businger *et al.* (1971). The equations for friction velocity (u_*), flux temperature (θ_*), and flux moisture (q_*) are given by

$$u_* = kV/[\ln(z/z_0) - \psi_M(z/L)], \quad (13)$$

$$\theta_* = k(\theta - \theta_{z_0})/[0.74(\ln(z/z_0) - \psi_H(z/L))], \quad (14)$$

$$q_* = k(q - q_{z_0})/[0.74(\ln(z/z_0) - \psi_H(z/L))], \quad (15)$$

where V is horizontal velocity, z/L a non-dimensional stability parameter, k the von Karman's constant, and θ_{z_0} and q_{z_0} the values of θ and q at surface roughness height, z_0 (Zilitnkevich, 1970). The Monin–Obukhov stability length, L, is defined as

$$L = \frac{\bar{\theta} u_*^2}{k g \theta_*}, \quad (16)$$

where $\bar{\theta}$ is the average air temperature near the surface. The surface roughness length, z_0, is specified over land surface, while it is calculated over water surface using Charnock's relationship (Clarke, 1970)

$$z_0 = 0.018\frac{u_*^2}{g}, \quad (17)$$

with a minimum value of 0.0015 cm imposed on the z_0.

Above the surface layer, a one-and-half order ($E - \varepsilon$) turbulence closure scheme, using two prognostic equations for the turbulent kinetic energy (E) and the turbulent energy dissipation (ε), is incorporated with the level 2.5 scheme of Mellor and Yamada (1982) to account for turbulent transport in the transition layer. The prognostic equations for the turbulent kinetic energy, E, and its dissipation, ε (Duynkerke and Driedonks, 1987) are given as (in the z-coordinate)

$$\frac{\partial E}{\partial t} = -V\cdot\nabla E + \left[-\overline{u'w'}\frac{\partial u}{\partial z} - \overline{v'w'}\frac{\partial v}{\partial z} + \frac{g}{\theta_0}\overline{w'\theta_v'}\right] - \frac{\overline{\partial w'(E' + p'/\rho_0)}}{\partial z} - \varepsilon, \quad (18)$$

$A_E \qquad S_E \qquad B_E \qquad T_E \qquad D_E$

and

$$\frac{\partial \varepsilon}{\partial t} = -V\cdot\nabla\varepsilon + c_1\frac{\varepsilon}{E}\left[-\overline{u'w'}\frac{\partial u}{\partial z} - \overline{v'w'}\frac{\partial v}{\partial z} + \frac{g}{\theta_0}\overline{w'\theta_v'}\right] + c_2\frac{\hat{c}}{\hat{c}z}K_M\frac{\partial \varepsilon}{\partial z} - c_3\frac{\varepsilon^2}{E}, \quad (19)$$

$A_\varepsilon \qquad S_\varepsilon \qquad B_\varepsilon \qquad T_\varepsilon \qquad D_\varepsilon$

where A is the advection term, S the shear production term, B the buoyancy term, T the turbulent transport term and D the dissipation term for turbulent kinetic energy and energy dissipation. The level 2.5 closure of Mellor and Yamada (1982) contains the same prognostic turbulent kinetic energy equation [equation (18)]. After considerable algebraic reduction, the final forms of eddy diffusivities for momentum, heat, and moisture in the level 2.5 formulation are expressed as

$$K_M = c_4\ell(2E)^{1/2}S_M, \quad (20)$$

$$K_\theta = K_q = c_4\ell(2E)^{1/2}S_H, \quad (21)$$

where the non-dimensional functions S_M and S_H are reported by Mellor and Yamada, 1982. Eddy mixing length, ℓ, is parameterized for different stability conditions in terms of the known variables (Huang and Raman, 1991). Similar formulations for ℓ were also used by many investigators (e.g. Andre *et al.*, 1978; Mellor and Yamada, 1982). In the above equations, c_1, c_2, c_3, and c_4 are closure constants.

To account for advection effects, a modified version of the Warming–Kutler–Lomax advection scheme (Warming *et al.*, 1973) is used in the horizontal and the quadratic upstream interpolation in the vertical, while all vertical diffusion terms are computed by a time-implicit scheme. At the lower boundary, a no-slip condition is imposed for the wind. The water surface temperature is fixed and the land surface temperature is computed during the integration using the force–restore method (Bhumralkar, 1975; Deardorff, 1978). Relative humidity for the land surface remains unchanged, but the air in contact with the water surface is assumed to be saturated. The hydrostatic equation is used to obtain the surface pressure from the known upper level pressure. At the upper boundary, a radiation boundary condition (Klemp and Durran, 1983) is used to determine the upper perturbation pressure. Prognostic variables (u, v, θ, q, q_c, and q_r) are computed by the prediction equations using the forward-upstream differencing scheme except for the vertical advection terms. For the prognostic variables (E and ε), zero gradient is used, since no turbulence flux is assumed at the upper boundary. At the lateral boundaries, Orlanski's radiation condition (Orlanski, 1976) with forward-upstream scheme (Miller and Thorpe, 1981) is applied to the prognostic variables (u, v, θ, q, q_c, and q_r). For the other variables, E and ε, zero gradient boundary condition is used at lateral boundaries.

2.2. *Monte Carlo dispersion model*

The Monte Carlo model used in study was originally developed by Zannetti (1981, 1984, 1986). The model simulates the dispersion of buoyant and dynamically passive pollutants in the atmosphere by means of a large ensemble of Lagrangian particles moving with pseudo-velocities. These pseudo-velocities simulate the effects of the two basic dispersion components: (1) transport due to the mean wind, and (2) diffusion due to the turbulent velocity fluctuations. The Monte Carlo model assigns a horizontal wind aligned local coordinate system for each particle at each time step based on the horizontal mean wind direction at the particle location. In this local coordinate system, the x-axis is chosen to coincide with the mean wind direction. The choice of x-axis in the mean wind direction simplifies the treatment of the cross correlation terms, since in this local reference system it can be assumed that only the cross correlation $\overline{u'w'}$ is non-zero. Particle positions are then computed from the following relations:

$$x(t + \Delta t) = x(t) + [\bar{u}(t) + u'(t)]\Delta t,$$
$$y(t + \Delta t) = y(t) + [v'(t)]\Delta t, \quad (22)$$
$$z(t + \Delta t) = z(t) + [\bar{w}(t) + w'(t)]\Delta t,$$

where $\bar{u}$ and $\bar{w}$ represent the horizontal mean and vertical velocity components obtained from the mesoscale model resolved east–west, north–south, and vertical velocity components, while u', v' and w' are the subgrid scale semi-random turbulent velocity fluctuations (in each of the three directions) whose statistics were derived from the mesoscale model predicted boundary layer parameters. Since the grid-scale meteorological variables are defined only on the mesoscale model grid mesh, a linear interpolation scheme is used to estimate their values at each particle location.

The semi-random turbulent velocity fluctuations are generated by the following Monte Carlo scheme:

$$u'(t + \Delta t) = \phi_1 u'(t) + u''(t + \Delta t),$$
$$v'(t + \Delta t) = \phi_2 v'(t) + v''(t + \Delta t), \quad (23)$$
$$w'(t + \Delta t) = \phi_3 w'(t) + \phi_4 u'(t + \Delta t) + w''(t + \Delta t),$$

where u'', v'' and w'' are purely random, independent, and uncorrelated turbulent velocity fluctuations (i.e. "white noise"). These random fluctuations are taken to be Gaussian with zero mean and the following variances:

$$\begin{aligned}\sigma^2_{u''} &= \sigma^2_{u'}(1-\phi_1^2),\\ \sigma^2_{v''} &= \sigma^2_{v'}(1-\phi_2^2),\\ \sigma^2_{w''} &= \sigma^2_{w'}(1-\phi_3^2)-\phi_4^2\sigma^2_{u'}-2\phi_1\phi_3\phi_4 R_{u'w'}\sigma_{u'}\sigma_{w'},\end{aligned} \tag{24}$$

where $\sigma_{u'}$, $\sigma_{v'}$ and $\sigma_{w'}$ are the turbulent velocity standard deviations. The use of Monte Carlo technique in particle models is particularly important, since it allows every particle to move independently. This provides a computational algorithm generally faster than deterministic computations, since no interacting forces need to be computed. The parameters ϕ_1, ϕ_2, ϕ_3, and ϕ_4 in equations (23) and (24) are computed using the following algebraic manipulations (see for more information Zannetti, 1990)

$$\begin{aligned}\phi_1 &= R_{u'},\\ \phi_2 &= R_{v'},\\ \phi_3 &= \frac{R_{w'}-R_{u'}R^2_{u'w'}}{1-R^2_{u'}R^2_{u'w'}},\\ \phi_4 &= \frac{R_{u'w'}\sigma_{w'}(1-R_{u'}R_{w'})}{\sigma_{u'}(1-R^2_{u'}R^2_{u'w'})},\end{aligned} \tag{25}$$

where $R_{u'}$, $R_{v'}$ and $R_{w'}$ are auto-correlation coefficients that are assumed to be exponential.

$$\begin{aligned}R_{u'}(\Delta t) &= \exp(-\Delta t/T^{u'}_{\mathrm{L}}),\\ R_{v'}(\Delta t) &= \exp(-\Delta t/T^{v'}_{\mathrm{L}}),\\ R_{w'}(\Delta t) &= \exp(-\Delta t/T^{w'}_{\mathrm{L}}),\end{aligned} \tag{26}$$

where $T^{u'}_{\mathrm{L}}$, $T^{v'}_{\mathrm{L}}$ and $T^{w'}_{\mathrm{L}}$ are Lagrangian integral time scales. The one required cross correlation coefficient, $R_{u'w'}$, is given by the following equation:

$$R_{u'w'} = -\frac{u_*^2}{\sigma_{u'}\sigma_{w'}}\left(1-\frac{z-z_0}{h_i-z_0}\right), \tag{27}$$

where z is the height under consideration, u_* friction velocity, z_0 surface roughness length, and h_i mixed layer height.

The Lagrangian turbulent statistics in each of the three local component directions need to be determined. Several different methods have been proposed for defining Lagrangian statistics, but none of them has been found totally satisfactory. The Monte Carlo model uses the following formulations suggested by Hanna (1982).

Unstable conditions:
Standard deviations:

$$\sigma_{u'} = \sigma_{v'} = u_*\left(12+0.5\frac{h_i}{|L|}\right)^{1/3}, \tag{28}$$

$$\sigma_{w'} = 0.96 w_*\left(\frac{3z}{h_i}-\frac{L}{h_i}\right)^{1/3} \quad \text{for } z < 0.03h_i, \tag{29}$$

$$\sigma_{w'} = w_*\min\left[0.96\left(\frac{3z}{h_i}-\frac{L}{h_i}\right)^{1/3};\ 0.763\left(\frac{z}{h_i}\right)^{0.175}\right] \quad \text{for } 0.03h_i < z < 0.4h_i, \tag{30}$$

$$\sigma_{w'} = 0.722 w_*\left(1-\frac{z}{h_i}\right)^{0.207} \quad \text{for } 0.4h_i < z < 0.96h_i, \tag{31}$$

$$\sigma_{w'} = 0.37 w_* \quad \text{for } 0.96h_i < z < h_i \tag{32}$$

Lagrangian time scales:

$$T^{u'}_{\mathrm{L}} = T^{v'}_{\mathrm{L}} = 0.15\frac{h_i}{\sigma_{u'}} \tag{33}$$

$$T^{w'}_{\mathrm{L}} = 0.1\times z\Big/\sigma_{w'}\left[0.55+0.38\frac{(z-z_0)}{L}\right] \quad \text{for } z < 0.1h_i \text{ and } (z-z_0) > -L, \tag{34}$$

$$T^{w'}_{\mathrm{L}} = 0.59\frac{z}{\sigma_{w'}} \quad \text{for } z < 0.1h_i \text{ and } (z-z_0) < -L. \tag{35}$$

$$T^{w'}_{\mathrm{L}} = 0.15\frac{h_i}{\sigma_{w'}}\left[1-\exp\left(-\frac{5z}{h_i}\right)\right] \quad \text{for } z > 0.1h_i. \tag{36}$$

Stable conditions:
Standard deviations:

$$\sigma_{u'} = 2.0u_*\left(1-\frac{z}{h_i}\right), \tag{37}$$

$$\sigma_{v'} = \sigma_{w'} = 1.3u_*\left(1-\frac{z}{h_i}\right). \tag{38}$$

Lagrangian time scales:

$$T^{u'}_{\mathrm{L}} = 0.15\frac{h_i}{\sigma_{u'}}\left(\frac{z}{h_i}\right)^{0.5} \tag{39}$$

$$T^{v'}_{\mathrm{L}} = 0.07\frac{h_i}{\sigma_{v'}}\left(\frac{z}{h_i}\right)^{0.5} \tag{40}$$

$$T^{w'}_{\mathrm{L}} = 0.1\frac{h_i}{\sigma_{w'}}\left(\frac{z}{h_i}\right)^{0.8} \tag{41}$$

Neutral conditions:
Standard deviations:

$$\sigma_{u'} = 2.0u_*\exp\left(-\frac{3fz}{u_*}\right), \tag{42}$$

$$\sigma_{v'} = \sigma_{w'} = 1.3u_*\exp\left(-\frac{2fz}{u_*}\right). \tag{43}$$

Lagrangian time scales:

$$T^{u'}_{\mathrm{L}} = T^{v'}_{\mathrm{L}} = T^{w'}_{\mathrm{L}} = \frac{0.5z}{\sigma_{w'}}\Big/\left(1+\frac{15fz}{u_*}\right), \tag{44}$$

where f is Coriolis parameter, u_* friction velocity, w_* convective velocity, h_i mixed layer height, L Monin–Obukhov length, and z_0 surface roughness length. All these boundary layer parameters (u_*, w_*, L, and z_0) are obtained from the mesoscale model, while the time variation of the mixed layer height (h_i) is determined from the time variation of the mesoscale model predicted turbulent kinetic energy (E).

The turbulent velocity standard deviations are determined using the following relationships for heights greater than the mixed layer height (Etling *et al.*, 1986):

$$\sigma_{u'} = \sigma_{v'} = 0.91E^{1/2}, \tag{45}$$

$$\sigma_w = 0.52E^{1/2}, \tag{46}$$

while the Lagrangian time scales are set to 600 and 30 s for the horizontal and vertical components, respectively (Gryning *et al.*, 1987). In the above equations, the mean turbulent kinetic energy (E) is obtained from the mesoscale model.

3. A BRIEF DESCRIPTION OF THE ACCIDENT

The Bhopal gas accident was one of the world's deadliest industrial disasters. The Union Carbide plant was licensed to manufacture phosgene, monomethyl amine, methyl isocyanate, and carbaryl. The plant is located due north of the Bhopal urban area. In the southwestern part of the plant, a relatively large

water body of Upper Lake is located. The accident occurred with the leakage of the methyl isocyanate gas from a nozzle at about 33 m height above the ground. The gas leak started around 0030 IST in the early hours of 3 December 1984, and continued for about 90 min until 0200 IST. The methyl isocyanate gas is twice as heavy as air and a reactive, toxic, flammable compound. The gas is known to attack the respiratory system, eyes, and skin. Investigative reports indicated that about 40 tons of the methyl isocyanate gas escaped into the atmosphere and affected all living beings and vegetation.

On the night of the episode, there were no recorded meteorological observations. According to the available reports and local residents, the episode occurred under stable atmospheric conditions. Night hours were marked by substantial suppression of turbulent diffusion. The ambient winds that night were near calm and mostly northwesterly and subsequently northerly. The other important parameter, mixed layer height was estimated as 200 m based on the mixed layer height values for New Delhi (Singh and Ghosh, 1985).

The only concentration-related observation was obtained by mapping the degree of damage to trees, crops and vegetables in different parts of the city. This was the best integrated concentration monitor available at that time. Several scientists from various organizations (mainly the Indian Agricultural Research Institute and the Central Board for the Prevention and Control of Water Pollution) tracked the path of the gas cloud and gauged the comparative exposure levels encountered. The extent of the vegetation damage obtained from this study is shown in Fig. 1 in terms of area in the affected zones. It was observed that all types of vegetation (from the top of the big trees to the ground level vegetation) were mostly affected in the eastern, southeastern and southern directions of the plant. The worst affected area was located southeast of the plant (J.P. Nagar colony). It was also observed that with increasing downwind travel distance from the Union Carbide plant, the damaging affect on the vegetation decreased considerably.

Since the methyl isocyanate gas is denser than air, one would expect that gravity slumping was important. However, according to Singh and Ghosh (1985), the conditions of the release, the chemical nature of the gas, and the observations on the damaged vegetation affected by the gas conclusively suggested that the gravity slumping was not at all important. For example, if the gravity slumping was important, the Union Carbide plant and its immediate vicinity would

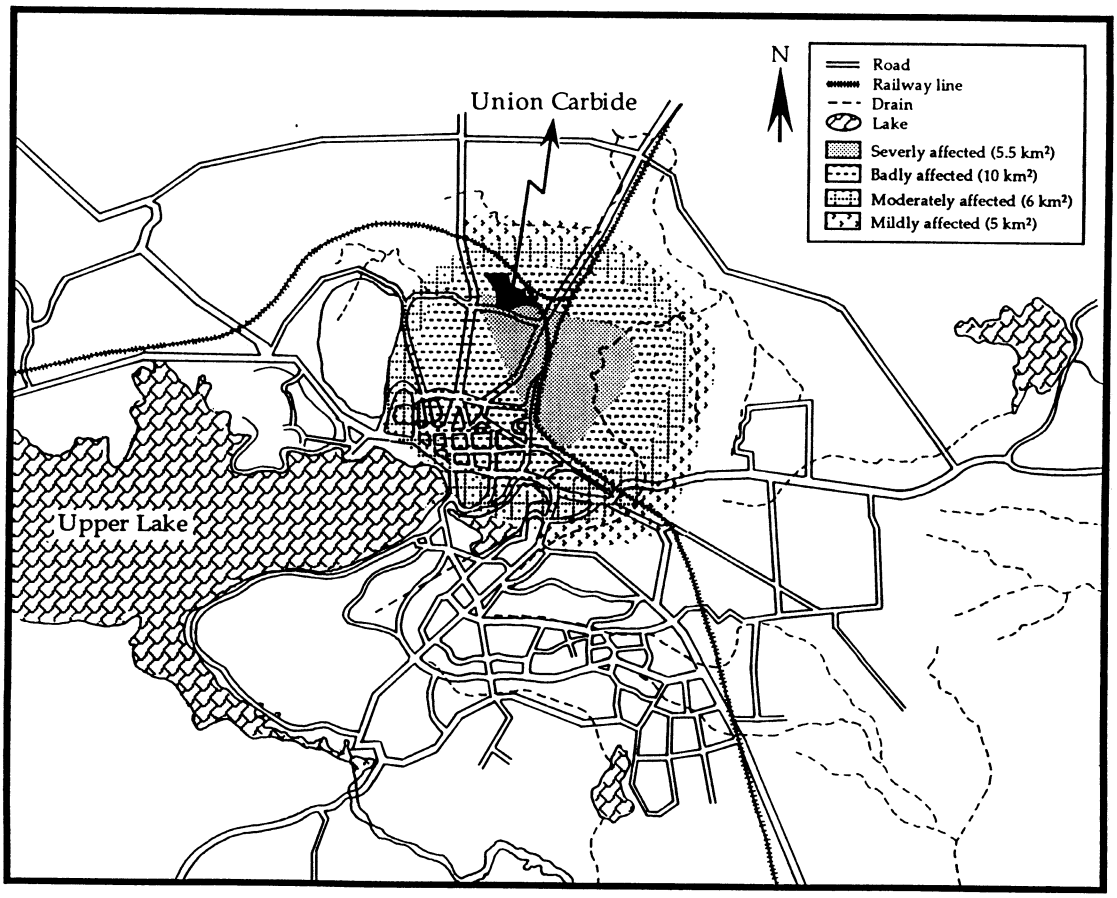

Fig. 1. Zones of influence of methyl isocyanate gas on vegetation, based on the average scores of damage to each species (after Singh and Ghosh, 1985).

Table 1. Description of the numerical experiments

Case description	Ambient flow ($m\,s^{-1}$)	Plume rise	Remarks
B1 Northwesterly winds	$U_g = 0.7$ $V_g = -0.7$	No	
B2 Northerly winds	$U_g = 0.0$ $V_g = -1.0$	No	
B3 Influence of Upper Lake	$U_g = 0.7$ $V_g = -0.7$	No	Upper Lake is removed
B4 Influence of Bhopal city	$U_g = 0.7$ $V_g = -0.7$	No	The urban area is removed
B5 Influence of plume rise	$U_g = 0.7$ $V_g = -0.7$	Yes	

have been the worst affected. However, this was not observed. Chemical scorching effects on the vegetation were only observed several hundred meters away from the plant. Methyl isocyanate gas is also thoroughly miscible in the air. It was reported that this property of the gas led to a rapid initial dilution of the gas. Therefore, the gravity slumping phase was missed altogether.

4. NUMERICAL EXPERIMENTS AND MODEL PARAMETERS

The numerical experiments were designed to investigate the role of the surface induced mesoscale circulations and various environmental parameters on the dispersion of methyl isocyanate gas. Due to unavailability of the meteorological observations on the night of the accident, the experiments were conducted based on mean climatological data. Topographical features were not considered, since Bhopal is surrounded by fairly flat terrain. Gravity slumping was neglected, since the initial dilution of the gas was so rapid that the gas cloud was carried away by the prevailing wind without showing any symptoms of gravity slumping. The numerical experiments include the influence of two observed ambient wind directions (northwesterly and northerly), Upper Lake, Bhopal's urban area, and plume rise. A complete description of the numerical experiments is given in Table 1.

Table 2 shows the mesoscale model parameters for the Bhopal simulations. The mesoscale model domain contains 14 non-uniform grid levels in the vertical and 35×30 grid points in the horizontal with a uniform grid interval of 1 km (Fig. 2). The use of a 1 km grid interval in the mesoscale model should not violate the hydrostatic assumption, since the stable night hours substantially suppressed the magnitude of the vertical acceleration. The model is integrated for 11 h after sunset (1800 IST) on 2 December 1984. Nocturnal boundary layers tend to be highly stable in the Bhopal region with relatively dry conditions associated with the northeasterly monsoon flow. Wind speeds tend to be low during this period. According to reports and local residents, the wind was nearly calm and the atmosphere was very stable on the night of the accident. An ambient flow of about $1\,m\,s^{-1}$ and a vertical potential temperature gradient of $6°C\,km^{-1}$ are adopted for all simulations. The initial surface temperatures are based on climatological observations. It was assumed that the surface temperature is 16°C over the rural area, while the temperature over the Bhopal urban area increases gradually to a maximum value of 22°C at the urban center. The Upper Lake surface temperature is assumed as 20°C and kept constant during the integration. Bhopal city is well built up towards the city center. The surface roughness values are assumed to be 12 cm over the urban center, decreasing to 7 cm towards the suburban area and 4 cm over the rural area.

Table 2. The mesoscale meteorological model parameters for the Bhopal simulations

Quantity	Value
Model start time	1800 IST
Day of year	2 December
Mean latitude	23°N
Model run time	11 h
Time step	15 s
Rural area surface temperature	16°C
Upper Lake surface temperature	20°C
Urban center surface temperature	22°C
Soil thermal diffusivity	$0.0018\,cm^2\,s^{-1}$
Geostrophic wind speed	$1\,m\,s^{-1}$
Potential temperature gradient	$6°C\,km^{-1}$
Relative humidity	50%
Horizontal grid spacing (Δx, Δy)	1 km
Grid domain size (x, y, z)	$35 \times 30 \times 14$
Rural area surface roughness	4 cm
Suburban area surface roughness	7 cm
Urban center surface roughness	12 cm
Model top	1 km
Vertical levels	0, 3, 33, 65, 100, 150, 200, 250, 300, 350, 400, 600, 800, 1000 m

Computationally, the mesoscale model provided three-dimensional wind and turbulence fields at 4 min intervals, and then the Monte Carlo model simulated the dispersion of methyl isocyanate gas using these wind and turbulence fields. The Monte Carlo model simulation began at 0030 IST and continued 4.5 h until 0500 IST on 3 December 1984. The pollution concentration is estimated based on the spatial distribution of the particles by simply counting the number of particles in a concentration calculation grid (Fig. 2). This estimate of concentration depends on the total number of particles and size of the grid cells. To obtain a statistically steady concentration field, it is

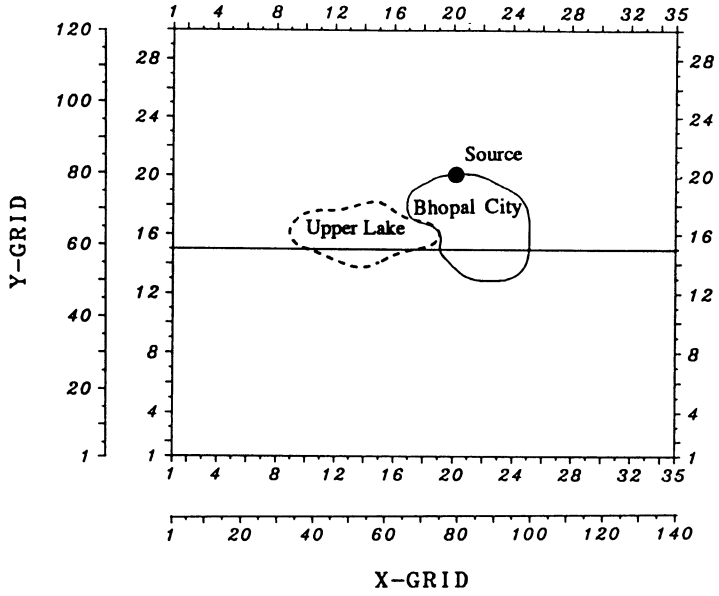

Fig. 2. Map of Bhopal area showing the location of Union Carbide plant, Bhopal city and Upper Lake. Tick marks (1–35 and 1–30) on the boundary show the mesoscale meteorological model grids and the marks (1–140 and 1–120) show the Monte Carlo dispersion model concentration calculation grids. The solid horizontal line marks the location of the vertical cross sections shown in Fig. 6.

Table 3. The Monte Carlo dispersion model parameters for the Bhopal simulations

Quantity	Value
Model start time	0030 IST
Day of year	3 December
Model run time	4.5 h
Time step	20 s
Emission start time	0030 IST
Emission stop time	0200 IST
Horizontal grid spacing (Δx, Δy)	250 m
Grid size (x, y, z)	140 × 120 × 17
Model top	400 m
Source height	33 m
Emission rate	7 kg s^{-1}
Total number of particles released	35,000

usually necessary to release a large number of particles of the order of several thousands. A total of 35,000 particles were released between 0030 IST and 0200 IST. Each released particle represents a discrete quantity of the total pollutant mass. Table 3 shows the Monte Carlo model parameters for the Bhopal simulations.

5. DISCUSSION OF RESULTS

5.1. *Case B1: influence of northwesterly winds*

The mesoscale model predicted horizontal potential temperature fields are shown in Fig. 3 at the source height 33 m after 2 and 7 h of simulation. Bhopal's urban area has different surface temperatures from those of the surrounding non-urban environs. Early at night (by the second hour), the closed isotherms over the city separate this area from the surrounding areas with a maximum value at the urban center and a large temperature gradient at the urban edge associated with the urban heat island. The spatial distribution of the isotherms over the Upper Lake area also indicates the development of a land breeze circulation. At night, the land surface and the air in contact with it cool off more rapidly than the lake water surface. This differential cooling generates a mesoscale circulation known as land breeze circulation.

Later at night (by the seventh hour), the northwesterly ambient winds advect the warm urban and lake air over relatively cooler rural areas along the downwind side of the city and the lake, thereby reducing the thermal gradient. Along the upwind side of the city and the lake, the ambient winds advect cooler rural air over relatively warmer urban and lake areas, causing a tighter gradient. As a result of the advection of the thermal gradient and the radiative cooling at night, the urban heat island intensity decreases. In contrast, land breeze circulation intensity slightly increases due to the differential cooling between the lake and the surrounding rural areas.

The mesoscale model predicted horizontal wind vector fields are shown in Fig. 4 at the source height 33 m after 2 and 7 h of simulation. Bhopal's urban area produces changes in the surface and atmospheric characteristics. For example, the urban heat island causes deformation of the pressure field over the city,

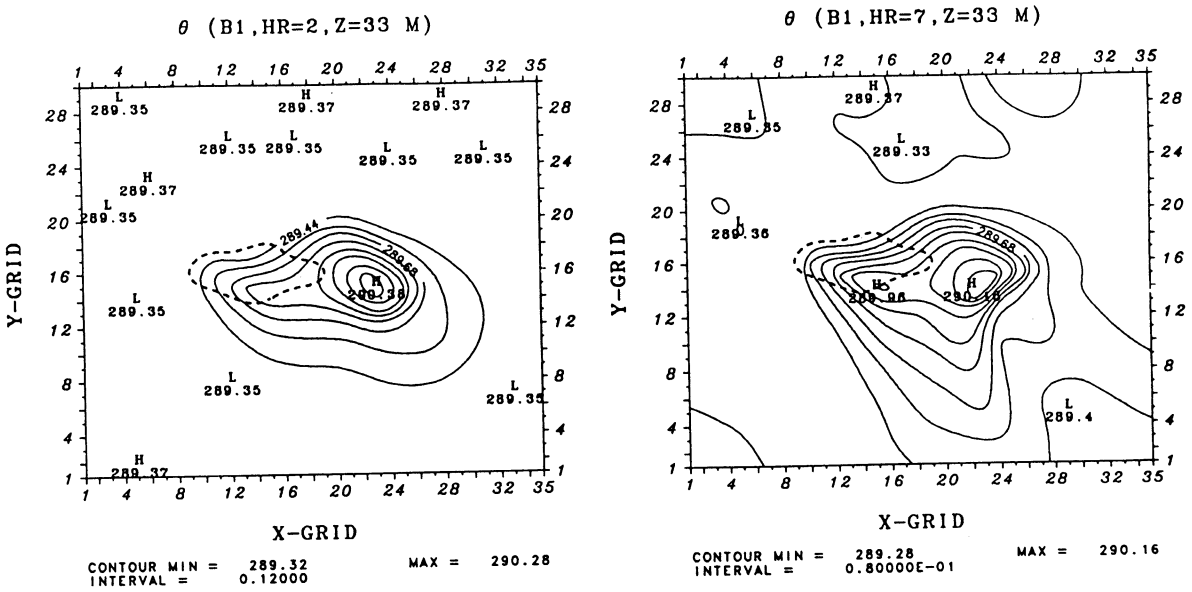

Fig. 3. The mesoscale meteorological model predicted horizontal potential temperature fields, θ(K), at source height 33 m after 2 and 7 h of simulation for the northwesterly wind case.

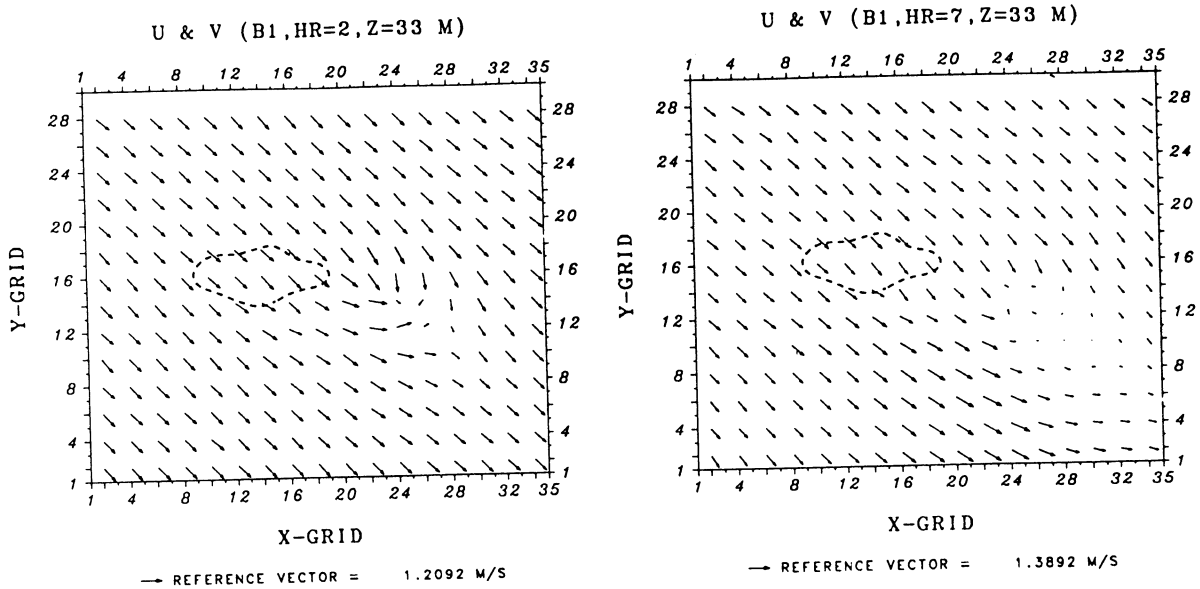

Fig. 4. The mesoscale meteorological model predicted horizontal wind vector fields, u and v(m s^{-1}), at source height 33 m after 2 and 7 h of simulation for the northwesterly wind case.

creating a lower pressure region. The rougher urban surface increases the frictional drag on the flow. Air traversing the area encounters these changes. Early at night, the horizontal winds converge southeast of the city and increase in speed due to the acceleration of the air toward the lower pressure region. This convergence region is later advected further downwind by the ambient winds. The advection of the convergence region is strongly controlled by the magnitude of the ambient wind and the intensity of the total heat input to the air. Additionally, Upper Lake causes its own mesoscale circulation because of its size. The horizontal winds tend to change their direction south of the lake associated with the land breeze circulation. However, this is not clear in the figure. Relatively strong urban heat island circulation must be suppressing strong development of the land breeze circulation. The interaction between these local circulations will be examined more closely in Cases B3 and B4.

Figure 5 shows the mesoscale model predicted vertical velocity fields at the source height 33 m after 2 and 7 h of simulation. In the figure, upward motion is represented by solid lines, while downward motion is represented by dashed lines. Their extremes are indicated by the letters H (High) and L (Low), respectively. Early at night, the thermally induced urban

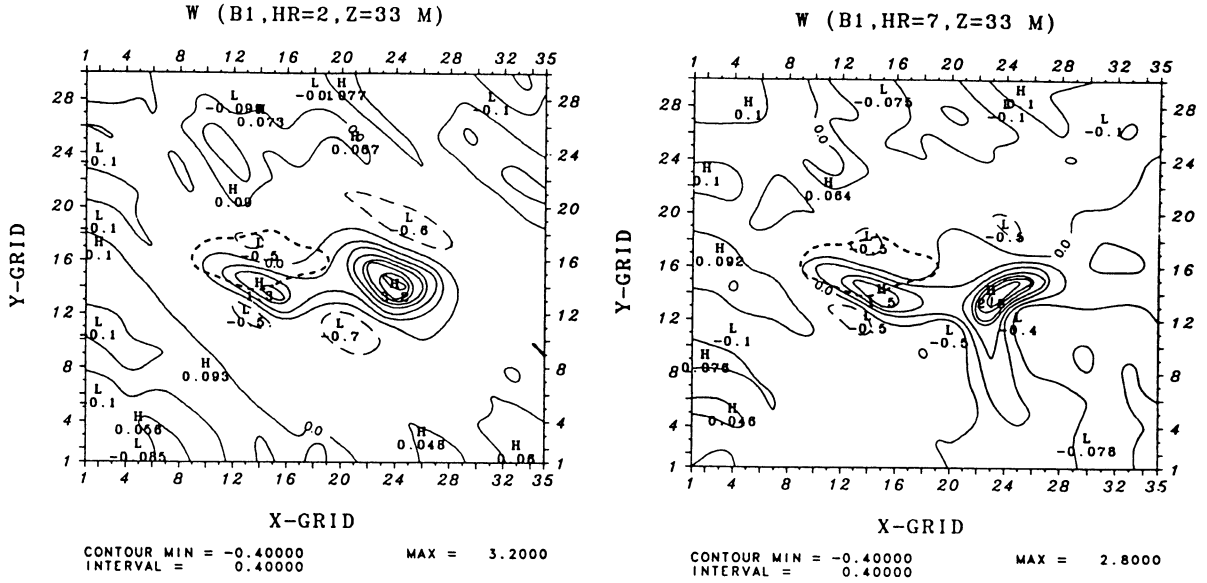

Fig. 5. The mesoscale meteorological model predicted vertical velocity fields, w (cm s^{-1}), at source height 33 m height after 2 and 7 h of simulation for the northwesterly wind case.

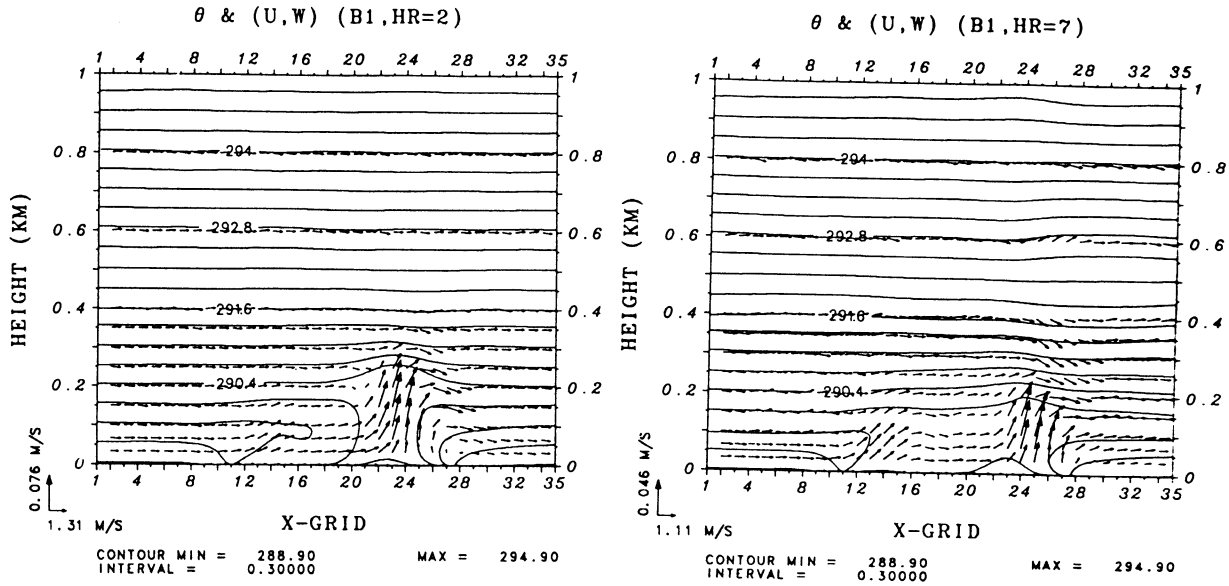

Fig. 6. The mesoscale meteorological model predicted vertical cross sections of the potential temperature, θ, and the wind vector fields, u and w (at Y-GRID No. 15 of Fig. 2) after 2 and 7 h of simulation for the northwesterly wind case. Maximum u and w are plotted at the left bottom corner of the figure.

heat island circulation is evidenced by an upward motion region over the city and downward motion regions surrounding the city in the general direction of the ambient wind. This circulation develops as the warm air over the city rises and expands. As the air expands, it cools and flows back toward the city at the edges of the urban area and thereby establishes a self-contained circulatory system. A similar circulation pattern associated with the land breeze circulation is also seen on the southern shore of Upper Lake. Later at night as the radiative cooling progresses, the intensity of both the upward and downward motions over the city decreases, while the intensity of the upward motion on the southern shore of the lake slightly increases.

Figure 6 shows the vertical sections of the mesoscale model predicted wind and potential temperature fields from another perspective. Early at night, the thermal structure shows the existence of a nocturnal stable atmosphere over non-urban areas. In moving over the urban area, the combination of the increased temperatures and the increased surface roughness produces major alterations. A well-defined urban boundary layer forms over the city and is capped by an elevated urban inversion layer aloft. The urban boundary layer and the inversion layer aloft result

from mechanical turbulence associated with the rougher urban surface, plus thermal turbulence associated with the relatively less stable atmosphere of the urban area. Both the mechanical turbulence and the thermal turbulence cause upward motion over the city and consequently downward motion surrounding the city. The urban boundary layer attains a depth of about 250 m by this hour and becomes more shallow further away from the city center.

Later at night, the urban heat island intensity decreases and strong stability suppresses turbulent mixing in the vertical direction. As a result, the boundary layer shrinks to a depth of about 200 m. Note that the predicted urban boundary layer height is in good agreement with the mixed layer height for Bhopal estimated by Singh and Ghosh (1985). A different behavior of the boundary layer structure over the Upper Lake area is also seen from the cross sections. Early at night, a shallow and stable marine boundary layer forms over the lake. This stable boundary layer is later deepened as the radiative cooling progresses at night.

The Monte Carlo model simulated dispersion of methyl isocyanate gas are shown in Figs 7 and 8 after 90, 150, 210 and 270 min of release. The results are presented in horizontal planes at the source height 33 m and near the surface, respectively. Advective and diffusive growth of the gas reflects the dramatic change in wind direction associated with the urban heat island circulation. The gas dispersion dominates southeast of the Union Carbide plant, where the worst effects of the accident were felt. Concentration values

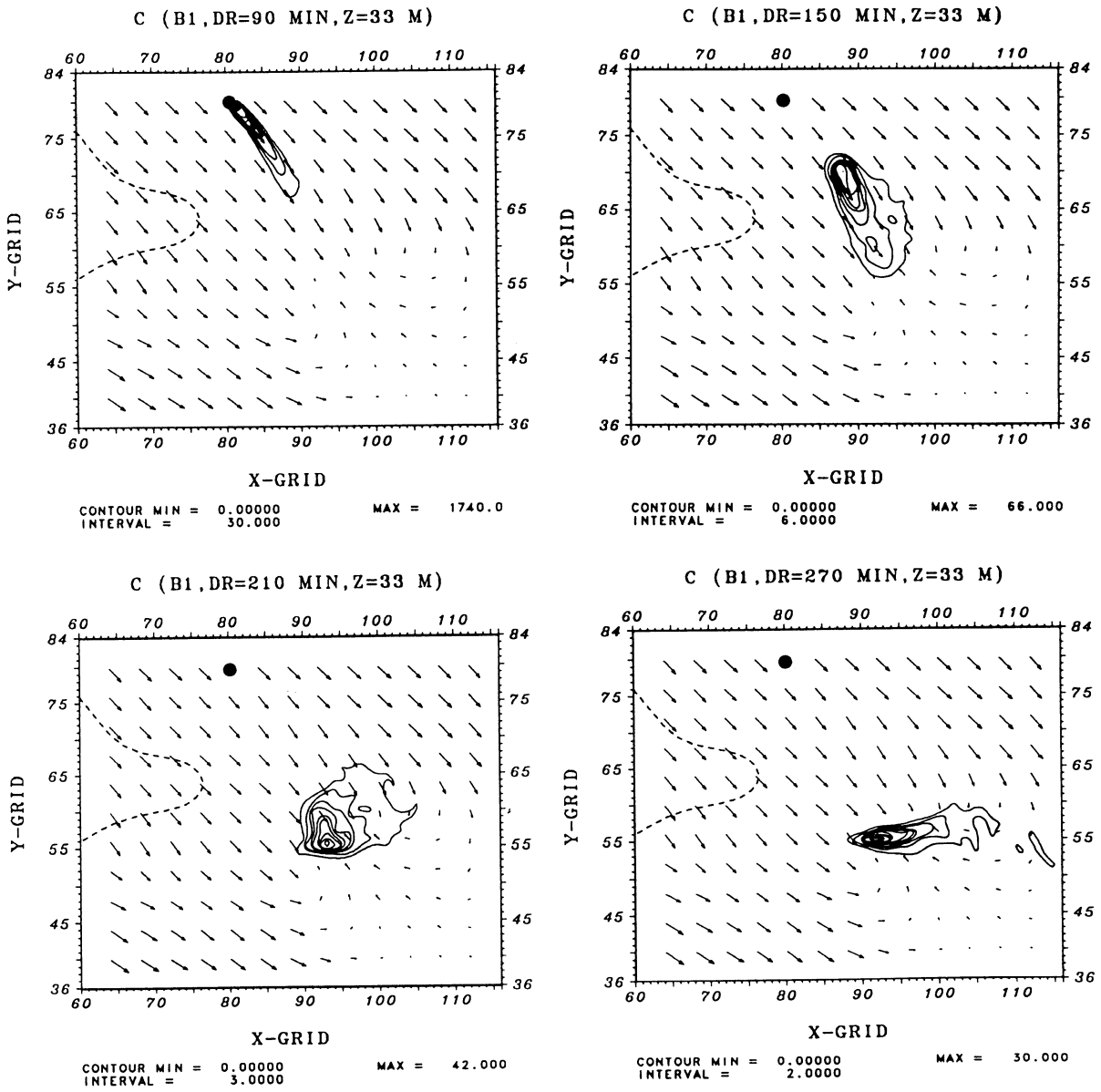

Fig. 7. The Monte Carlo dispersion model predicted source height concentration fields, $C(10^3\ \mu g\,m^{-3})$, superimposed on the mesoscale meteorological model predicted wind vector fields after 90, 150, 210 and 270 min of travel with northwesterly wind. The location of the Union Carbide plant is indicated by a dot.

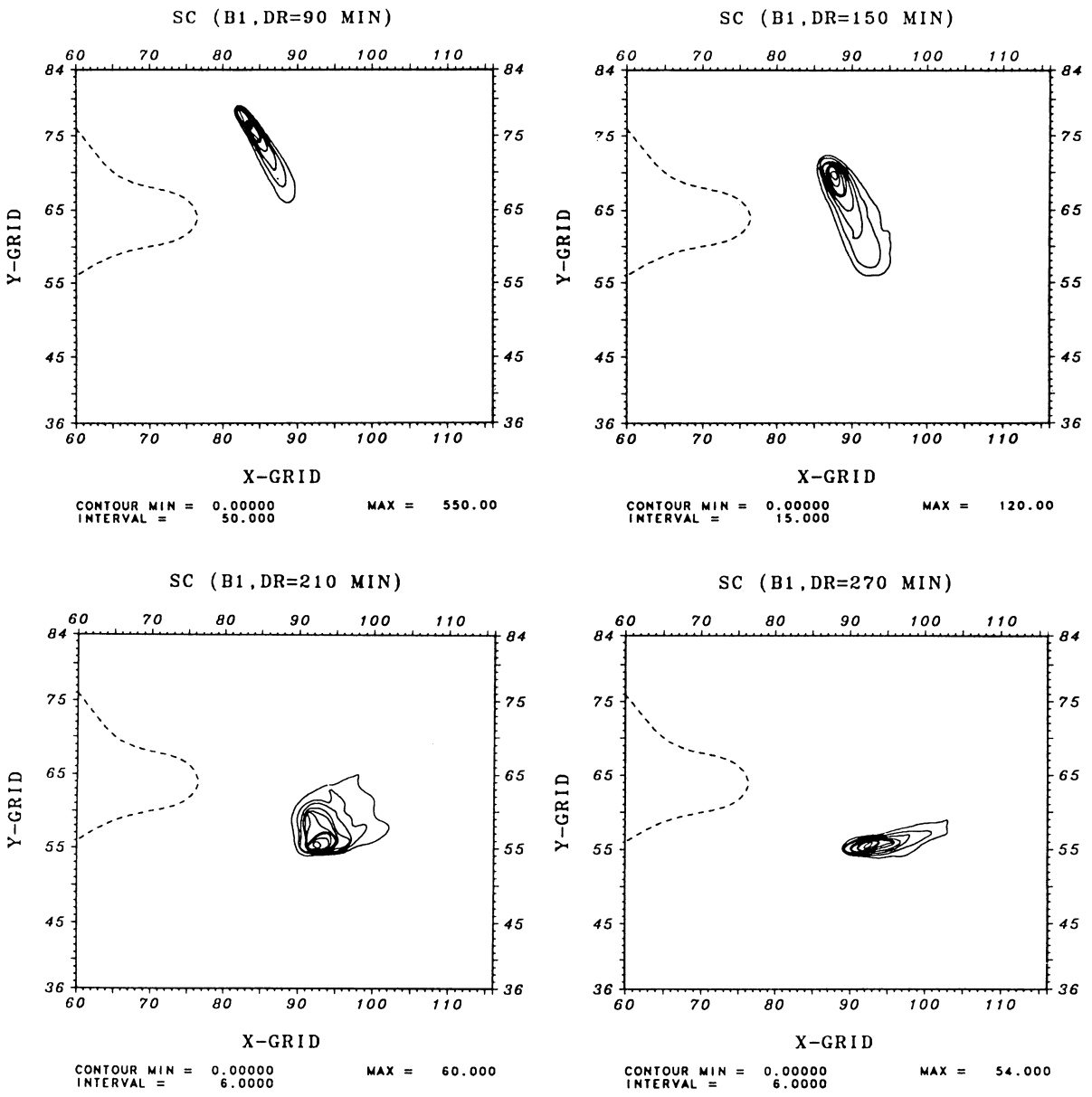

Fig. 8. The Monte Carlo dispersion model predicted near surface concentration fields, $SC(10^3\ \mu g\,m^{-3})$, after 90, 150, 210 and 270 min of travel with northwesterly wind.

both at the source height and near the surface decrease with increasing downwind travel distance as the gas cloud continues to expand and disperse over a larger area.

After 90 min of release, gas emission stops and the gas cloud moves towards the urban center with little mixing occurring. Concentration values near the surface directly beneath the moving gas cloud are thus lower than those at the source height. After 150 min of release, the results show that the circulation and thermodynamic structure of the Bhopal urban area significantly affects the gas dispersion. The gas cloud diffuses within the urban area due to the turbulent mixing caused by the weaker stability and higher surface roughness elements of the city. Fumigation resulting from the weaker stability of the urban area leads to significant increases in the computed concentration values near the surface. After 210 and 270 min of release (3.5 and 4.5 h after initial release), the influence of the urban heat island on the gas dispersion is more pronounced. The gas cloud both at the source height and near the surface is trapped over the city by the return flow of the urban heat island circulation, instead of being advected farther downwind. The rapid decrease in the magnitude of the concentrations from 90 to 150 min is also slowed down by the upward mass diffusion via turbulent mixing.

Figure 9 shows vertical cross sections of the gas dispersion in an east–west plane constructed through the locations of high concentration regions (*Y*-GRID = 77, 69, 56 and 55 of Fig. 7(a)–(d), respectively). The cross sections show weak vertical mixing after 90 min of release. High concentrations are therefore seen within a relatively shallow layer near the surface.

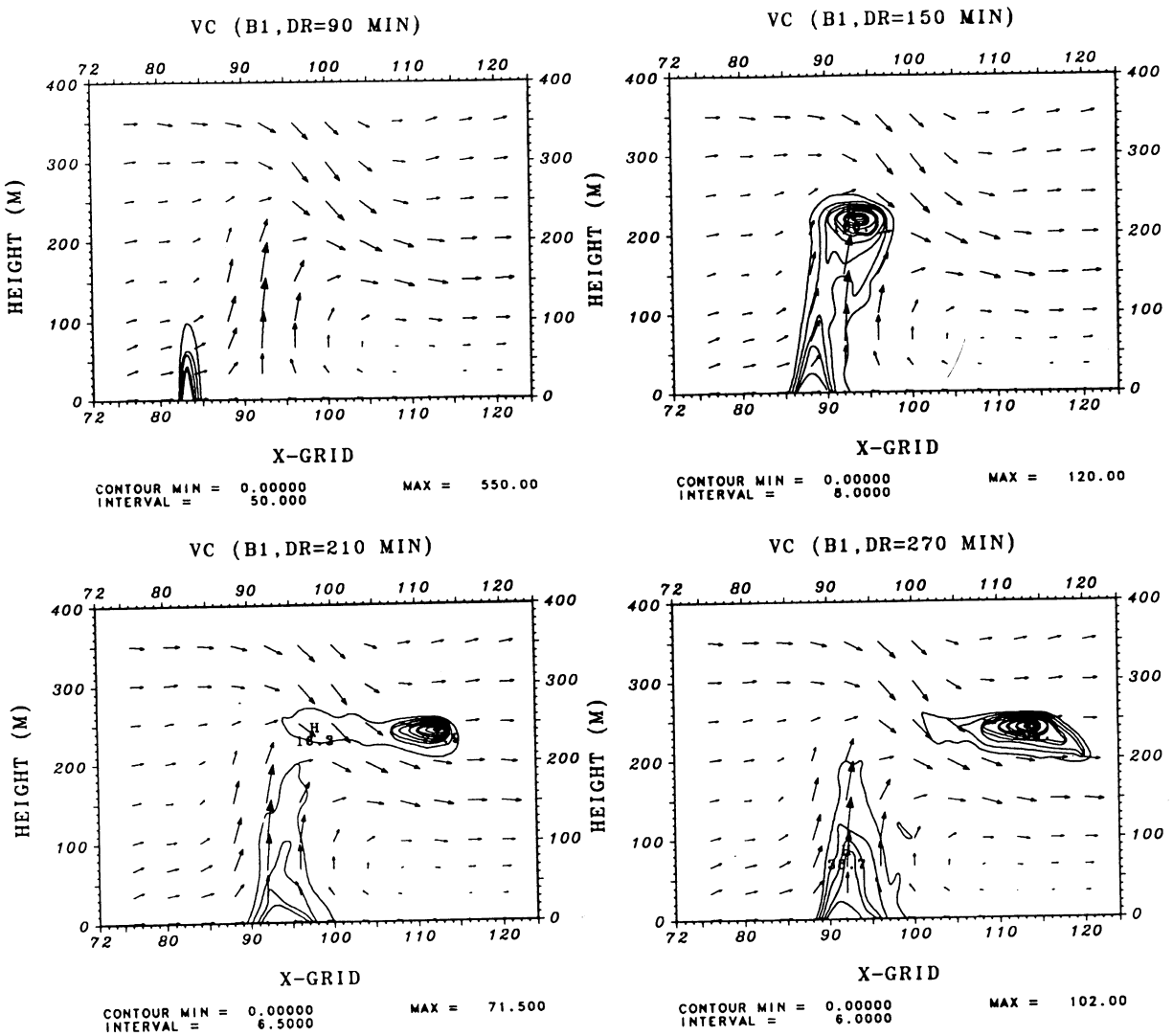

Fig. 9. The Monte Carlo dispersion model predicted vertical cross sections of the concentration fields, VC (10^3 $\mu g\,m^{-3}$), after 90, 150, 210 and 270 min of travel with northwesterly wind.

After 150 min of release, the gas cloud is mixed upward within the urban area via turbulent mixing. Upward dispersion of the gas is retarded at the top of the urban boundary layer by the elevated urban inversion layer. The gas cloud is thus confined to the first 250 m depth above the surface. Later (after 210 min of release), the gas cloud axis is curved and tilted downstream, resulting in a different advection rate of the gas cloud at the top of the urban boundary layer.

The results of this case study suggest that the reported complex dispersion of the gas at Bhopal could have resulted from the interaction of thermally forced mesoscale circulations and that the impact of the accidentally released methyl isocyanate gas occurred within a small area southeast of the Union Carbide plant. In this area, the gas cloud is confined over Bhopal city by the return flow of the urban heat island circulation for a significant time period (at least until sunrise). The results also suggest that the concentration values decrease with increasing travel distance, thereby indicating that the effect of the gas diminishes with increasing distance.

The reported and observed dispersion pattern of the gas generally seems to support these findings. For example, Singh and Ghosh (1985, 1987) reported that the worst affected area was located southeast of the plant (J. P. Nagar colony). This colony was engulfed with copious dense white fumes having a bitter sweet smell. The gas concentration was so high that visibility was very poor. The gas cloud lingered over the J. P. Nagar colony for an unusually long time (about 5 h after the start of the release), resulting in a large number of casualties by the time the smoky pall was cleared at about 0530 IST. It was also observed that with increasing downwind travel distance from the Union Carbide plant, the damaging effect of the gas on the vegetation decreased considerably.

5.2. *Case B2: influence of northerly winds*

This case study examines the influence of the other observed wind direction on the gas dispersion. All prescribed model parameters are the same as those of Case B1, except that wind direction is now from the north.

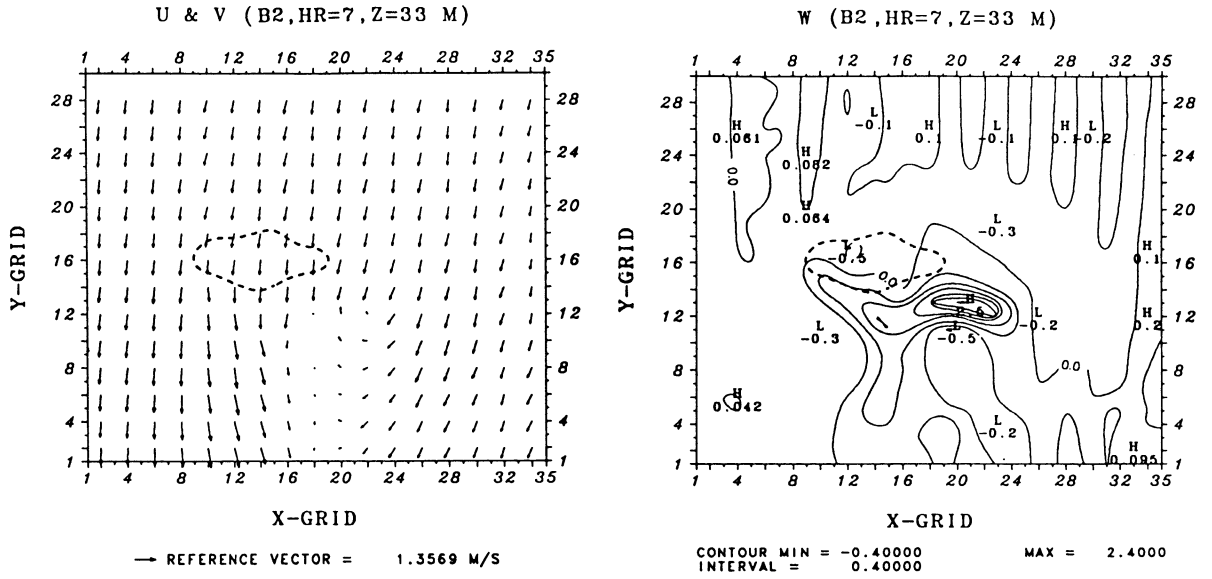

Fig. 10. The mesoscale meteorological model predicted horizontal wind vector field, u and v (m s^{-1}), and vertical velocity field, w(cm s^{-1}), at source height 33 m after 7 h of simulation for the northerly wind case.

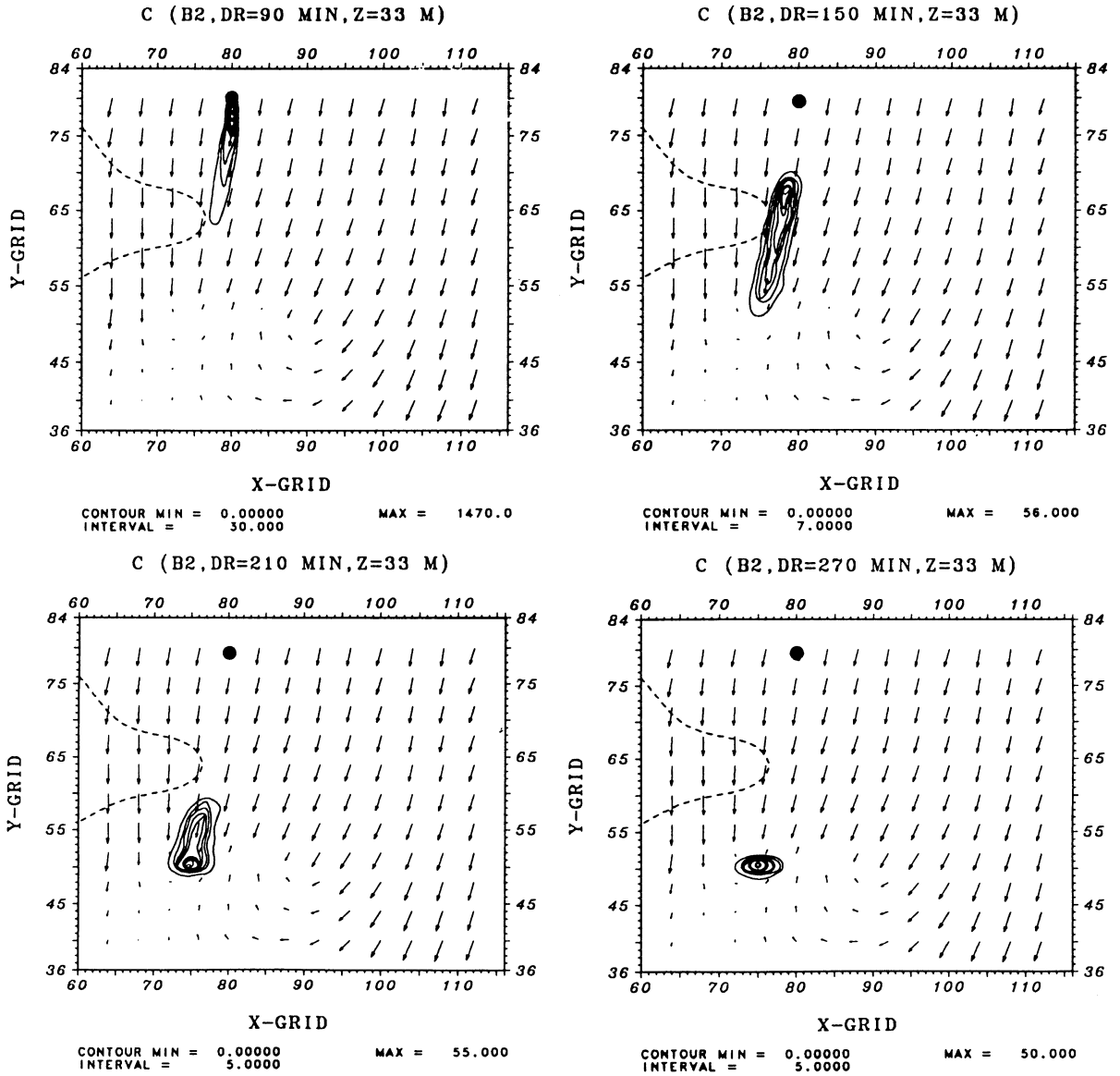

Fig. 11. Same as in Fig. 7, except for the northerly wind case.

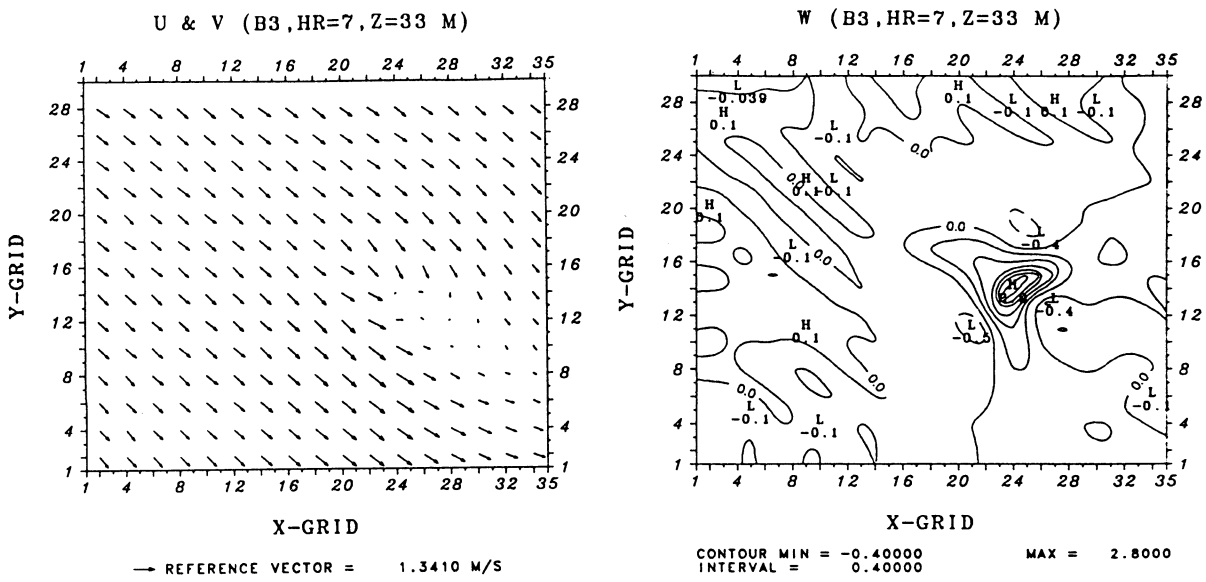

Fig. 12. Same as in Fig. 10, except for the northwesterly wind case with Upper Lake removed from simulation domain.

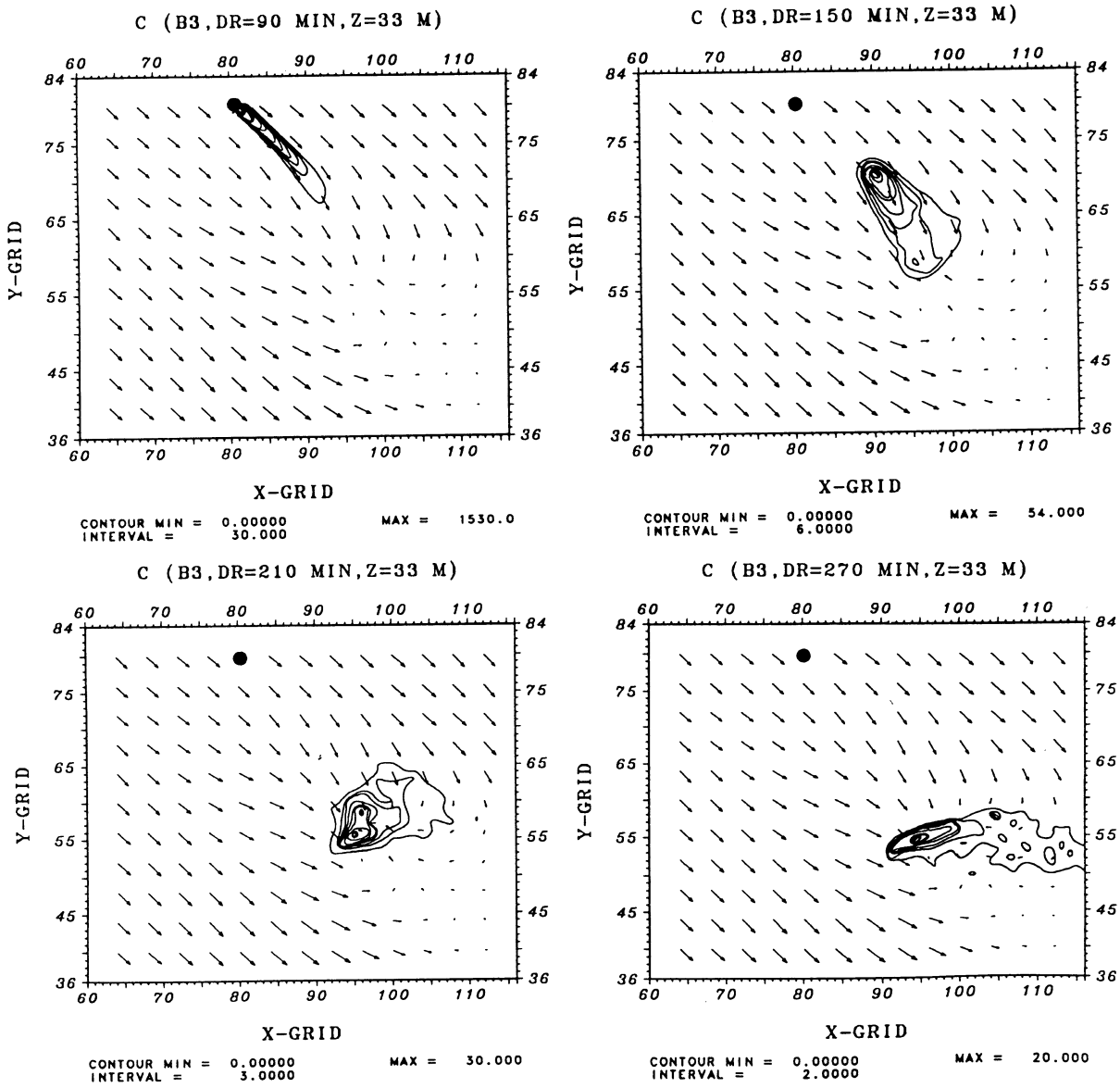

Fig. 13. Same as in Fig. 7, except that Upper Lake is removed from simulation domain.

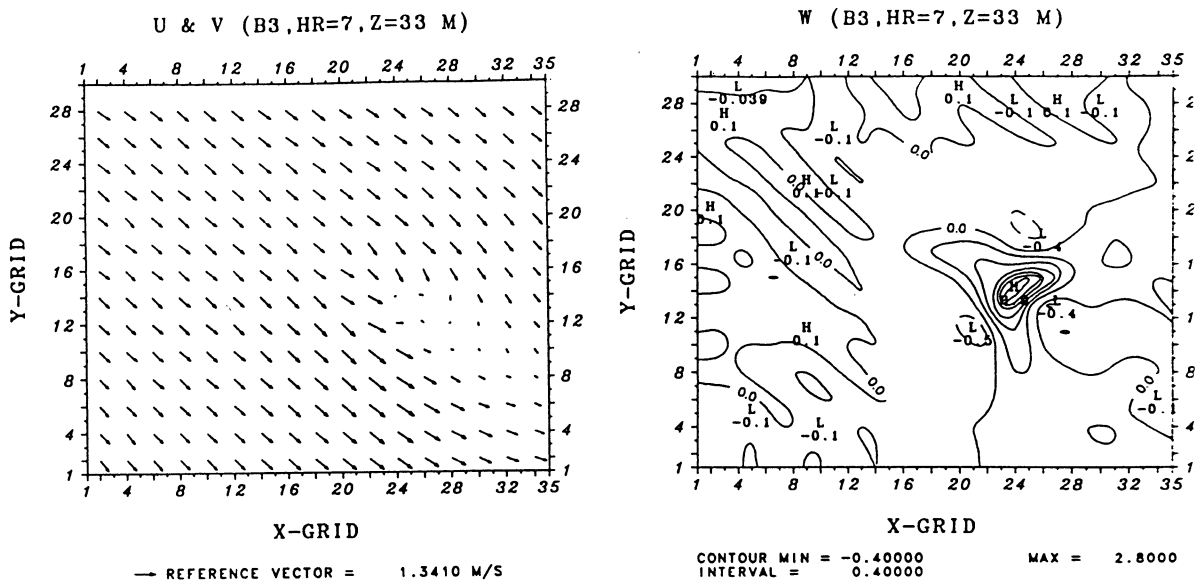

Fig. 12. Same as in Fig. 10, except for the northwesterly wind case with Upper Lake removed from simulation domai

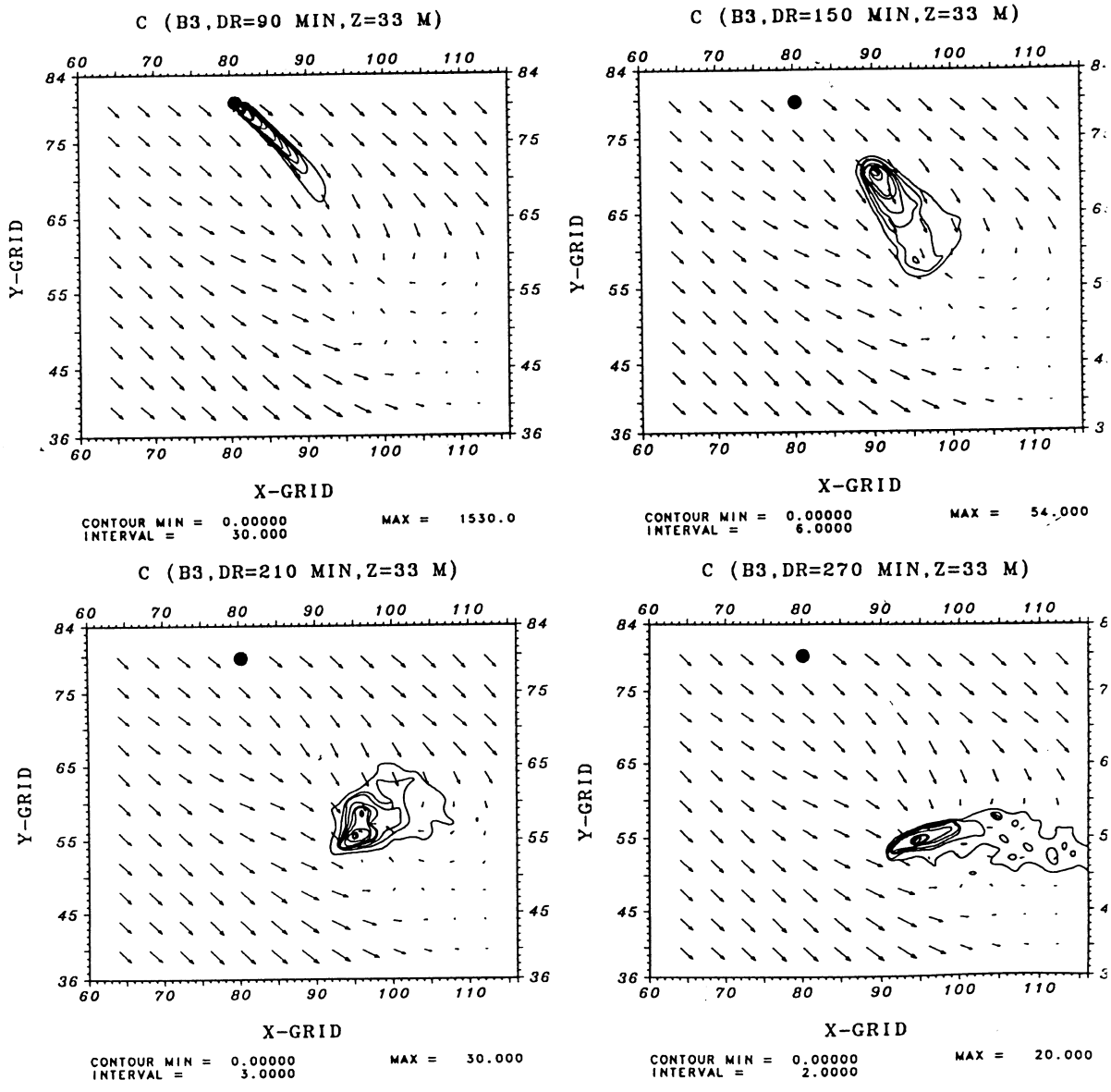

Fig. 13. Same as in Fig. 7, except that Upper Lake is removed from simulation domain.

Figure 10 shows the horizontal wind vector field and vertical velocity field at the source height 33 m after 7 h of simulation. In contrast to Case B1, the horizontal winds converge south of Bhopal city. A comparison of vertical velocity field with that from Case B1 shows that the upward motion regions over both the city and the lake appear to merge under the northerly winds and that the magnitude of the vertical velocities are less than those of Case B1. It appears that the shift in wind direction from northwest to north increases the interaction between the local circulations (the urban heat island and the land breeze). Advective and diffusive growth of the gas responds to the change in the wind direction. The change causes a general shift in the orientation of the gas cloud (Fig. 11). The gas cloud is now advected over the suburban and lake areas and trapped south of the city. The northerly flow direction also causes a general narrowing of the released gas cloud and a strengthening of the concentration gradient.

5.3. *Case B3: influence of Upper Lake*

Upper Lake is the most prominent geographical feature in the Bhopal area. At night, the land surface and the air in contact with it cool off more rapidly than the lake water surface, and this differential cooling generates a land breeze circulation. In particular during the winter season, land breeze circulation reaches its maximum development. This case study examines the influence of Upper Lake on the gas dispersion. All prescribed parameters are kept identical to those of Case B1, except that Upper Lake is removed from the calculation domain.

Figure 12 shows horizontal wind vector field and vertical velocity field after 7 h of simulation. In contrast to Case B1, horizontal winds do not change their directions south of the lake. The vertical velocity field indicates that the extent and intensity of the urban heat island circulation seem to be modified slightly in the absence of Upper Lake from the calculation domain. As a result, the gas cloud disperses over a slightly larger area (Fig. 13) and therefore the concentration values are less than corresponding values from Case B1. This case study suggests that the extent and intensity of the urban heat island circulation and hence the gas dispersion could have been modified by the relatively large water body of Upper Lake.

5.4. *Case B4: influence of Bhopal city*

Previous case studies indicated that the circulation and thermodynamic structure of the Bhopal urban area significantly effects pollutant transport and diffusion. To further study the influence of the Bhopal urban area on the gas dispersion, all the prescribed parameters are again kept identical to those of Case B1, except that the Bhopal urban area is removed from the calculation domain.

Figure 14 shows the mesoscale model predicted horizontal wind vector field and vertical velocity field at the source height after 7 h of simulation. Substantial differences occur between the results of Case B1 and Case B4. The convergence region formed southeast of the city in Case B1 is not present in this case. Also, the land breeze circulation is seen more clearly from the changes in the wind direction south of the lake (this was not clear in Fig. 4 of Case B1). Another major difference between the two cases occurs in the predicted vertical velocity field. The vertical velocities on the southern shore of the lake are stronger in this case. These results indicate that the urban heat island circulation suppressed strong development of the land breeze circulation in Case B1. Advective and diffusive

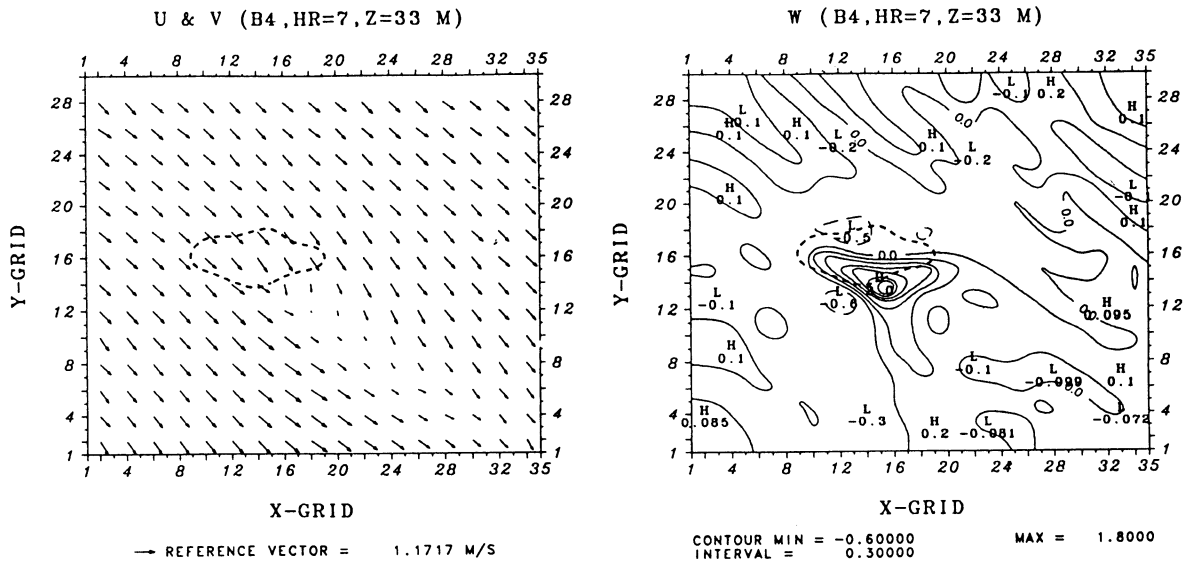

Fig. 14. Same as in Fig. 10, except for the northwesterly wind case with the Bhopal urban area removed from simulation domain.

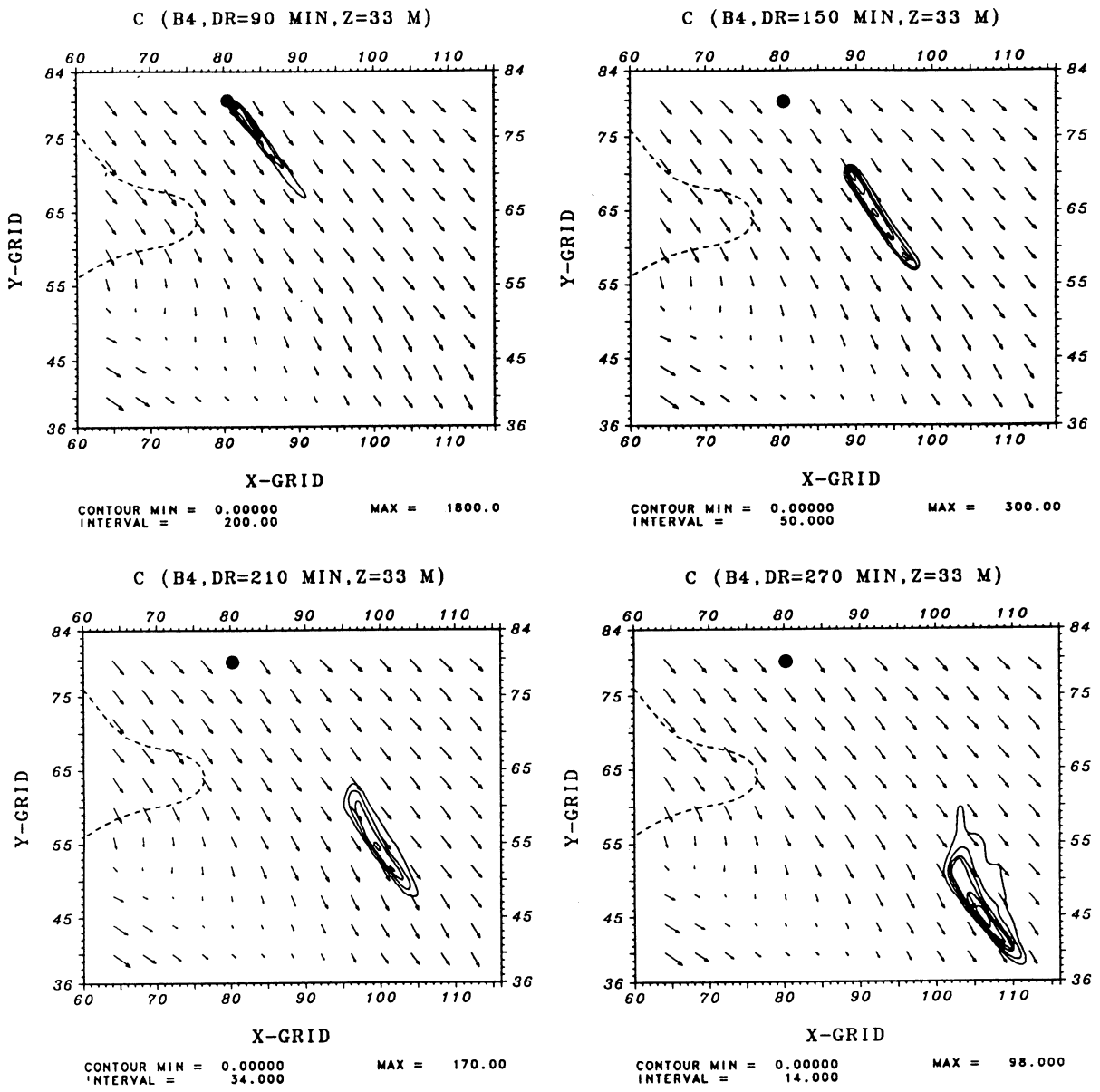

Fig. 15. Same as in Fig. 7, except that the Bhopal urban area is removed from simulation domain.

growth of the gas also reflects the influence of the Bhopal urban area. The gas cloud now exhibits less diffusion (Fig. 15) and therefore the concentration values at given travel times are higher than those of Case B1. The total horizontal distance traveled by the gas cloud is also increased in this case, since there is no return flow from the urban heat island circulation.

5.5. *Case B5: influence of plume rise*

Various reports on the accident indicated that the gas was ejected from the nozzle with a high speed. It was estimated that the exit velocity of the gas was on the order of 88 $m\,s^{-1}$ and that the nozzle's inside diameter was about 0.2 m. This case study examines the influence of plume rise on the gas dispersion. All prescribed parameters are identical to those of Case B1, except that plume rise calculation is included. The plume rise formulations used in this study are reported by Anfossi (1985).

Figure 16 shows the dispersion of methyl isocyanate gas with the inclusion of the plume rise. Although the dispersion patterns of the gas are similar to those of Case B1, differences occur in the magnitude of the concentrations. During at least the first 150 min of travel time, the stack height concentration values are less than those of Case B1, due to the dilution of the gas cloud by plume rise. After 210 and 270 min of release, the concentration values become identical to those of Case B1, due to the turbulent mixing. These results indicate that the influence of plume rise on the gas dispersion was important only in the first few kilometers downwind. Farther away from the plant, the influence of the plume rise on the gas dispersion is diminished.

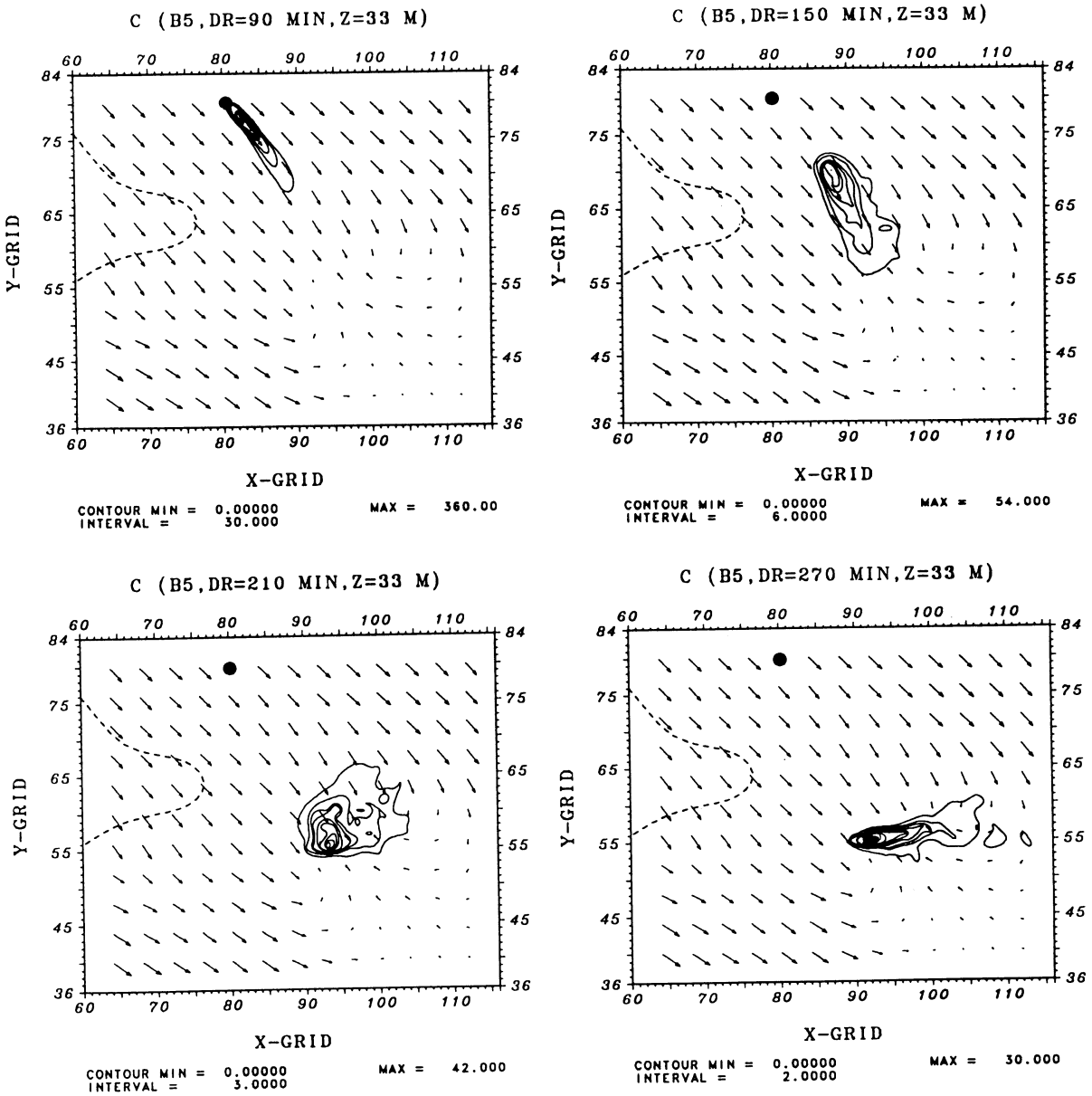

Fig. 16. Same as in Fig. 7, except that plume rise calculation is included in this case.

6. CONCLUSIONS

Two numerical models were coupled in this study; a three-dimensional mesoscale meteorological model and a three-dimensional Monte Carlo dispersion model. The dispersion of methyl isocyanate gas from the Bhopal accident was then investigated using the coupled models. A series of numerical experiments were performed to examine the possible role of the surface induced mesoscale circulations and various environmental parameters on this industrial gas episode.

The results of the numerical experiments suggest that the reported complex dispersion of the gas at Bhopal could have resulted from the interaction of thermally forced local mesoscale circulations. The results especially point to the effect of the Bhopal urban heat island which dominated the local circulation and trapped the gas cloud over Bhopal city for a significant time period (at least until sunrise). The extent and intensity of the Bhopal urban heat island circulation and hence the gas dispersion also appears to be modified by the relatively large water body of Upper Lake around the city. Occurrence of the accident during calm winds, clear skies and stable nighttime atmospheric conditions that prevailed during the accident are consistent with the formation of the surface induced local circulation effect in Bhopal.

The results of the experiments also suggest that the gas dispersion occurs within a small area southeast of the Union Carbide plant, where the worst effects of the accident were felt. In this area, simulated concentration values decreased with increasing downwind travel distance, thereby suggesting that the effect of the gas diminished with the increase in the distance traveled. Finally, the results also suggest that the

influence of plume rise was important only over the first few kilometers downwind. However, farther away from the plant, the effect of the plume rise on the gas dispersion diminished.

Acknowledgements—The authors wish to thank Professor M. P. Singh for his valuable assistance in providing observations and several helpful suggestions. We would also like to thank Professor R. D. Bornstein for several helpful discussions. This work was supported by the Division of International Programs of the National Science Foundation under Grant ATM-9008926.

Disclaimer—The opinions presented herein are those of the authors alone and should not be interpreted as necessarily those of Failure Analysis Associates, Inc. (FaAA).

REFERENCES

Andre J. C., de Moor G., Lacarrere P., Therry G. and du Vachat R. (1978) Modeling the 24-hour evaluation of the mean and the turbulent structures of the planetary boundary layer. *J. atmos. Sci.* **35,** 1861–1883.

Anfossi D. (1985) Analysis of plume rise data from five TVA steam plants. *J. Clim. appl. Met.* **24**(11), 1225–1236.

Artz R., Pielke R. A. and Gallowat J. (1985) Comparison of the ARL/ATAD constant level and the NCAR isentropic trajectory analyses for selected case studies. *Atmospheric Environment* **19,** 47–63.

Bhumralkar C. M. (1975) Numerical experiments on the computation of ground surface temperature in atmospheric general circulation model. *J. appl. Met.* **14,** 1246–1258.

Bornstein R. D., Pechinger U., Miller R., Klotz S. and Street R. L. (1987a) Modeling the polluted coastal urban environment. Volume 1: PBL model. EPRI Report EA-5091 for Contract No. 1630–13, 172 pp.

Bornstein R. D., Pechinger U., Salvador R., Shieh L. J. and Ludwig F. (1987b) Modeling the polluted coastal urban environment. Volume 2: Dispersion model. EPRI Report EA-5091 for Contract No. 1630–13, 153 pp.

Boybeyi Z. and Raman S. (1992a) A three-dimensional numerical sensitivity study of convection over the Florida peninsula. *Boundary-Layer Met.* **60,** 325–359.

Boybeyi Z. and Raman S. (1992b) A three-dimensional numerical sensitivity study of mesoscale circulations induced by circular lakes. *Met. Atmos. Phys.* **49,** 19–41.

Businger J. A., Wyngaard J. C., Izumi Y. and Bradley E. F. (1971) Flux-profile relationships in the atmospheric surface layer. *J. atmos. Sci.* **28,** 181–189.

Clarke R. H. (1970) Recommended methods for the treatment of the boundary layer in numerical models. *Aust. Met. Mag.* **18,** 51–73.

Deardorff J. W. (1978) Efficient prediction of ground surface temperature and moisture with inclusion of a layer of vegetation. *J. geophys. Res.* **83C,** 1889–1903.

Duynkerke P. G. and Driedonks A. G. M. (1987) A model for the turbulent structure of the stratocumulus-topped atmospheric boundary layer. *J. atmos. Sci.* **44,** 43–64.

Etling D., Preuss J. and Wamser M. (1986) Application of random walk model to turbulent diffusion in complex terrain. *Atmospheric Environment* **20,** 741–747.

Gryning S. E., Holtslag A. M., Irwin J. S. and Sivertsen B. (1987) Applied dispersion modeling based on meteorological scaling parameters. *Atmospheric Environment* **21,** 79–89.

Hanna S. R. (1982) Applications in modeling. In *Atmospheric Turbulence and Air Pollution Modeling* (edited by Nieuwstadt F. T. M. and Van Dop H.), pp. 275–310. D. Reidel, Dordrecht.

Huang C. Y. and Raman S. (1990) Numerical simulations of cold air advection over the Appalachian Mountains and the Gulf Stream. *Mon. Weath. Rev.* **118,** 343–362.

Huang C. Y. and Raman S. (1991) Numerical simulation of January 28 cold air outbreak during "GALE" I, the model and sensitivity tests of turbulence closures. *Boundary-Layer Met.* **55,** 381–407.

Klemp J. B. and Durran D. R. (1983) An upper boundary condition permitting internal gravity wave radiation in numerical mesoscale model. *Mon. Weath. Rev.* **111,** 430–444.

McNider R. T., Moran M. D. and Pielke R. A. (1988) Influence of diurnal and inertial boundary layer oscillations on long-range dispersion. *Atmospheric Environment* **22,** 2445–2462.

Mellor G. L. and Yamada T. (1982) Development of a turbulence closure model for geophysical fluid problems. *Rev. Geophys. Space Phys.* **20,** 851–875.

Miller M. J. and Thorpe A. J. (1981) Radiation conditions for the lateral boundaries of limited area numerical models. *Q. J. R. met. Soc.* **107,** 615–628.

Orlanski I. (1976) A simple boundary condition for unbounded hyperbolic flows. *J. Comput. Phys.* **21,** 251–269.

Pack D. H., Ferber G. J., Heffter J. L., Telegadas K., Angell J. K., Hoecker W. H. and Machta L. (1978) Meteorology of long range transport. *Atmospheric Environment* **12,** 425–444.

Pitts R. O. and Lyons T. J. (1992) A coupled mesoscale particle model applied to an urban area. *Atmospheric Environment* **26B,** 279–289.

Singh M. P. and Ghosh S. (1985) Perspectives in air pollution modeling with special reference to the Bhopal gas tragedy. Centre for Advanced Studies (CAS) Tech. Report, IIT, New Delhi.

Singh M. P. and Ghosh S. (1987) Bhopal gas tragedy: model simulation of dispersion scenario. *J. hazard. Mat.* **17,** 1–22.

Warming R. F., Kutler P. and Lomax H. (1973) Second- and third-order non-centered difference schemes for nonlinear hyperbolic equations. *AIAA J.* **11,** 189–196.

Zannetti P. (1981) Some aspects of Monte-Carlo type modeling of atmospheric diffusion. Preprints of the 7th AMS Conference on Probability and Statistics in Atmospheric Sciences, Monterey, CA, November 1978.

Zannetti P. (1984) A new Monte-Carlo scheme for simulating Lagrangian particle diffusion with wind shear effects. *Appl. Math. Modeling* **8,** 188–192.

Zannetti P. (1986) Monte-Carlo simulation of auto- and cross-correlated turbulent velocity fluctuations (MCLAGPAR II Model). *Environ. Software* **1,** 26–30.

Zannetti P. (1990) *Air Pollution Modeling*, 444 pp. Van Nostrand Reinhold, New York.

Zilitnkevich S. S. (1970) *Dynamics of the Atmospheric Boundary Layer*. Hydrometeorol, Leningrad.